Continental pollution in the Western Mediterranean basin: vertical profiles of aerosol and trace gases measured over the sea during TRAQA 2012 and SAFMED 2013

C. Di Biagio[1], L. Doppler[2,3,4], C. Gaimoz[1], N. Grand[1], G. Ancellet[2], J.-C. Raut[2], M. Beekmann[1], A. Borbon[1], K. Sartelet[5], J.-L. Attié[6,7], F. Ravetta[2], and P. Formenti[1]

(*corresponding author: claudia.dibiagio@lisa.u-pec.fr)

[1] *LISA, UMR CNRS 7583, Université Paris Est Créteil et Université Paris Diderot, Institut Pierre Simon Laplace, Créteil, France*

[2] *Sorbonne Universités, UPMC Univ. Paris 06; Université Versailles St-Quentin; CNRS/INSU, LATMOS-IPSL, Paris, France*

[3] *Freie Universität Berlin, Berlin, Germany*

[4] *Deutscher Wetterdienst, Metorological Observatory Lindenberg, Germany*

[5] *CEREA, Joint Laboratory École des Ponts ParisTech – EDF R & D, Université Paris-Est, 77455 Marne la Vallée, France*

[6] *Laboratoire d'Aérologie, University of Toulouse, UMR 5560 CNRS, France*

[7] *CNRM GAME UMR 3589 CNRS, METEO-FRANCE*

Abstract

In this study we present airborne observations of aerosol and trace gases obtained over the sea in the Western Mediterranean basin during the TRAQA (TRansport and Air QuAlity) and SAFMED (Secondary Aerosol Formation in the MEDiterranean) campaigns in summers 2012 and 2013. A total of 23 vertical profiles were measured up to 5000 m above sea level over an extended area

(40°-45°N latitude and 2°W-12°E longitude) including the Gulf of Genoa, Southern France, the Gulf of Lion, and the Spanish coast. During TRAQA and SAFMED the study area experienced a wide range of meteorological conditions which favoured the pollution export from different sources located around the basin. Also, several events of dust outflows were measured during the campaigns. Observations from the present study show that continental pollution largely affects the Western Mediterranean both close to coastal regions and in the open sea as far as ~250 km from the coastline. The measured aerosol scattering coefficient varies between ~20 and 120 Mm^{-1}, while carbon monoxide (CO) and ozone (O_3) mixing ratios are in the range of 60-165 ppbv and 30-85 ppbv, respectively. Pollution reaches 3000-4000 m in altitude and presents a very complex and highly stratified structure characterized by fresh and aged layers both in the boundary layer and in the free troposphere. Within pollution plumes the measured particle concentration in the Aitken (0.004-0.1 μm) and accumulation (0.1-1.0 μm) modes is between ~30 and 5000-6000 scm^{-3} (standard cm^{-3}), which is comparable to the aerosol concentration measured in continental areas under pollution conditions. Additionally, our measurements indicate the presence of highly concentrated Aitken layers (10000-15000 scm^{-3}) observed both close to the surface and in the free troposphere, possibly linked to the influence of new particle formation (NPF) episodes over the basin.

1. Introduction

Atmospheric aerosols play an important role on climate through their participation to several chemical, dynamical, and radiative processes. At present, still large uncertainties persist in the estimation of the aerosol direct and indirect effects mainly due to the difficulty of fully characterizing their spatial and vertical distribution and properties (Boucher et al., 2013).

The Mediterranean region is a complex area where atmospheric aerosols of different origins and types may be found (Pace et al., 2006; Kallos et al., 2007; Gkikas et al., 2012). High levels of

anthropogenic aerosol particles and pollutants are measured in the Mediterranean (Lelieveld et al., 2002), which is also indicated as one of the main hot spots for air quality issues (Monks et al., 2009).

The North-Western part of the Mediterranean basin, due to its proximity to highly polluted industrialized areas (such as the Po Valley in northern Italy and the Fos/Berre in southern France) and large coastal cities (Barcelona, Genoa, Marseilles, Nice, or Valencia), is frequently affected by continental outflows and severe pollution episodes (Mallet et al., 2005; Pérez et al., 2008; Pey et al., 2010). The strength of these episodes is particularly intense during summer when stable meteorological conditions and the high level of insolation promote photochemical reactions and the build-up of ozone and other pollutants (e.g. Millán et al., 2000).

A number of studies have investigated the dynamics of pollution export over the Western basin with the aim of characterizing the impact of anthropogenic emissions over this region. Most of these studies have been conducted in continental coastal areas and provide information on the vertical distribution of aerosols and their properties mainly close to local pollution sources. They include ground-based observations with lidars (Soriano et al., 2001; Pérez et al., 2004; Ancellet and Ravetta, 2005), and airborne campaigns, such as MECAPIP (MEso-meteorological Cycles of Air Pollution in the Iberian Peninsula) and RACAPMA (RegionAl Cycles of Air Pollution in the west central Mediterranean Area) in coastal Spain (Millán et al., 1996 and 1997), and ESCOMPTE (Experience sur Site pour Contraindre les Modeles de Pollution atmospherique et de Transport d'Emissions) in Southern France (Drobinski et al., 2007). The results of these studies have highlighted the important role of pollution in modulating the atmospheric composition in this part of the basin, as well as the high variability of the aerosol distribution and properties in link to different export conditions (Flamant and Pelon, 1996; Soriano et al., 2001; Mallet et al., 2005). In particular, the interaction between synoptic circulation and local dynamics, such as orography and sea breezes, has been shown to strongly impact the vertical distribution, layering, and aging of

particles along coastal regions (e.g. Millan et al., 1997; Gangoiti et al., 2001; Pérez et al., 2004; Velchev et al., 2011).

The capability of reproducing this complexity by air quality models represents a real challenge (Jimenez et al., 2006; Jiménez-Guerrero et al., 2008), and experimental observations gives a fundamental support to test the performances of the model outputs over the Western Mediterranean environment.

The large set of observations conducted in the last decades in the Western Mediterranean has permitted mostly to characterise the dynamics and processes of pollution export in the surroundings of the basin. However, at the present time we miss an extensive representation of the mean load, distribution, and physico-chemical and optical properties of the atmospheric aerosols, as well as trace gases distribution, in the whole region, in particular over the remote sea. In addition, there is a significant lack of observations over some key areas, as for example the Gulf of Genoa, directly under the influence of the outflow from the highly polluted Po Valley (Velchev et al., 2011).

In this study we present measurements of aerosols and trace gas vertical profiles acquired during 24 scientific flights performed with the ATR-42 French research aircraft during the TRAQA (TRansport and Air QuAlity) and SAFMED (Secondary Aerosol Formation in the MEDiterranean) campaigns in summers 2012 and 2013 in the framework of the Chemistry-Aerosol Mediterranean Experiment (CHARMEX, https://charmex.lsce.ipsl.fr/). The TRAQA and SAFMED flights explored an extended region of the Western Mediterranean basin between 40°-45°N latitude and 2°W-12°E longitude including the Gulf of Genoa, Southern France, the Gulf of Lion, and the Spanish coasts. Measurements were performed over the sea at various distances from the coastline with lidar and in situ instruments. During TRAQA and SAFMED the Western basin was under diverse synoptic conditions which led to the occurrence of different pollution export regimes (Mistral/Tramontane events, outflow from the Po Valley and the Iberian Peninsula) and allowed sampling atmospheric aerosols of different origin and types.

The main objective of the present work is to provide observations of the vertical distribution of aerosols and trace gases related to the export of anthropogenic pollution at the regional scale of the Western Mediterranean basin. The detailed knowledge of the vertical structure of the atmosphere is very important to understand the impact of continental pollution over the basin.

The paper is organized as follows: in Sections 2, 3, and 4 we describe the flight trajectories and strategy during TRAQA and SAFMED, the in situ measurements carried out on board the ATR-42 aircraft, and the meteorological conditions observed during the campaigns. In Sect. 5 we present the results. The aerosol and trace gases vertical profiles are shown in Sections 5.1 and 5.2. Section 5.3 is dedicated to analyse the variability of the pollution plume composition and atmospheric structure also in link with the different outflow conditions. Airborne measurements in presence of layers with high concentrations of fine particles are discussed in Section 5.4. The main conclusions are reported in Section 6.

2. Overview over flights

Figure 1 shows the trajectories of the flights performed during the TRAQA (20 June-13 July 2012) and the SAFMED (24 July-1 August 2013) campaigns. Research flights were performed with the SAFIRE (Service des Avions Français Instruments pour la Recherche en Environnement, http://www.safire.fr/) tropospheric aircraft ATR-42. The aircraft has a maximum endurance of 4 h. The flight altitude ranges between a minimum of ~60 m over the sea, to a maximum of ~5000 m above sea level (a.s.l.). The aircraft was based in Toulouse (43°36’N, 1°26’E, France) during TRAQA and in Genoa (44°24’N, 8°55’E, Italy) during SAFMED. Twenty-four flights for a total of ~75 hours of data have been collected. Seventeen of the twenty-four flights presented in the paper were performed during TRAQA (flight numbers V16 to V32) and 7 during SAFMED (V46 to V52). All flights were carried out during daytime, when light-induced chemistry favours the pollution levels. Frequently, two flights per day, with intermediate stops in different airports in

Southern France, Corsica, and Sardinia, were performed. The majority of flights were over the sea, with some exceptions investigating inland areas in Southern France and central Italy. Main information concerning the TRAQA and SAFMED flights is summarized in Table 1.

The general flight strategy consisted in plane flights with lidar observations and vertical ascents/descents to sound the vertical atmospheric column (from ~60-100 m to 3000-5000 m a.s.l.) and identify main meteorological and aerosol features, followed by straight levelled runs (SLRs) within the detected aerosol layers. In this study we focus on vertical profiles data. A total of 23 profiles were acquired in 20-30 minutes each by performing a spiral trajectory ~10-20 km wide. Fig. 1 also identifies the geographical position of each sounding. As shown in Fig. 1 the profiles were performed at different distances from the coastline, from a minimum of ~5-10 km for V31 and V32 to more than ~250 km for V20 and V25, and covered almost all the different sectors of the Western basin.

3. Measurements and methods

The basic equipment of the ATR-42 aircraft includes sensors for the measurements of meteorological parameters (pressure, temperature, relative humidity, wind components), radiative fluxes (down- and up-welling shortwave and longwave radiation), and carbon monoxide (CO) and ozone (O_3) mixing ratios.

Aerosol sampling was performed using the AVIRAD system (Formenti et al., 2011). AVIRAD is an iso-axial and iso-kinetic inlet which, at the normal cruise speed of the ATR-42 (~93 m s^{-1}), samples air at a volumetric flow of ~350 l min^{-1}. The 50% passing efficiency of the inlet was tested to be 12 μm diameter. Various sampling lines depart from AVIRAD to connect to different instruments mounted inside the aircraft cabin: (i) a 3-wavelength nephelometer (TSI Inc., model 3563) for the measurement of the dry particle volume total scattering (σ_s) and hemispherical backscattering (σ_{bs}) coefficients at 450, 550, and 700 nm; (ii) a 7-wavelengths aethalometer (Magee Sci., model AE31)

149 for the measurement of the particle absorption coefficient (σ_a) at 370, 470, 520, 590, 660, 880, and
150 950 nm; (iii) an optical particle spectrometer (GRIMM Inc., model 1.129) for the measurement of
151 the particle number concentration over 32 size classes between 0.3 and 32 μm in diameter; (iv) a
152 Condensation Particle Counter (CPC, TSI Inc., model 3775) for the measurement of the total
153 particle number concentration in the diameter range 0.004-3.0 μm; and (v) 3 lines for aerosol
154 sampling on filter membranes and a 4-stage cascade impactor (Dekati Inc) to measure the bulk and
155 size-segregated particle composition. In addition, the ATR-42 was equipped with a Passive Cavity
156 Aerosol Spectrometer Probe (PCASP, model 100X) optical particle spectrometer for the
157 measurement of the aerosol number concentration over 31 size classes between 0.1–3.0 μm. The
158 PCASP was installed outside the cabin on the left side of the aircraft fuselage.

159 In this study we consider measurements of the (i) aerosol scattering coefficient from the
160 nephelometer, (ii) particle concentration from the CPC and PCASP instruments (GRIMM data are
161 not considered since they are available only below ~350 m during TRAQA), (iii) CO and O_3 trace
162 gases from the MOZART analyser, and (iv) meteorological parameters from the ATR-42 sensors. A
163 more detailed description of the nephelometer, CPC, PCASP, and MOZART measurements and
164 their data analysis is provided in the following sections.

165 The present analysis is based only on measurements obtained in cloud free conditions.

166

167 **3.1 Aerosol scattering coefficient**

168 A three-wavelength integrating nephelometer has been used to measure the dry particle volume
169 total scattering (σ_s) coefficient at 450, 550, and 700 nm. The sampling flow rate was 30 l min^{-1}.
170 Data were acquired at 6 s resolution during TRAQA and 1 s resolution during SAFMED. The
171 instrument was calibrated prior to each campaign with free-particle air and CO_2 as gases of low and
172 high known scattering coefficient. Nephelometer measurements have been corrected for angular
173 truncation and Lambertian non-idealities by applying the formulae by Anderson and Ogren (1998).

The measurement uncertainty on σ_s is calculated taking into account for the photon counting, gas calibration, and angular corrections uncertainties (Anderson et al., 1996; Anderson and Ogreen, 1998). The total uncertainty on σ_s is estimated to be lower than 10% at the three wavelengths.

The nephelometer measured the scattering coefficient in dry air conditions. This is due to the heating of the airflow while entering the aircraft cabin and the temperature in the cavity of the instrument. The relative humidity measured during the flights inside the nephelometer was <25% in more than ninety percent of cases, with values up to ~40% occasionally observed at very low altitudes (<200 m) over the sea surface. A possible underestimation of the scattering coefficient may thus occur in case of hygroscopic aerosols, especially under high relative humidity conditions in the atmosphere.

The particle scattering Ångström exponent (α_s) has been calculated from spectral nephelometer measurements with a power-law fit of the measured scattering coefficients versus wavelength.

3.2 Aerosol particle number concentration

The vertical profiles of the total particle number concentration in the Aitken (dN_{Aitken}, 0.004-0.1 µm), accumulation (dN_{Acc}, 0.1-1.0 µm) and coarse (dN_{Coarse}, >1.0 µm) modes have been obtained by combining CPC and PCASP data. The CPC and the PCASP measured at a sample flow of 1.5 and 0.06 l min^{-1}, respectively, and with a time resolution of 1 s for the PCASP and 5 s and 1 s for the CPC during TRAQA and SAFMED, respectively.

The PCASP was factory calibrated with monodisperse polystyrene sphere latex (PSL) whose complex refractive index at the instrument operating wavelengths (632.8 nm) is 1.59-0i. The measured sphere-equivalent optical diameter has been converted to a sphere-equivalent geometrical diameter (D_g) by taking into account the complex refractive index of the sampled aerosol (Liu and Daum, 2000). Given that in the very large majority of cases the aerosol sampling during TRAQA

198 and SAFMED was associated to the export of pollution plumes, only pollution aerosols have been
199 considered for PCASP correction. Note that these data are not optimized for dust or marine aerosol
200 observations. A large interval of values (n~1.50-1.72, k~0.001-0.1 for UV-visible wavelengths) are
201 reported in the literature for the real and the imaginary parts of the refractive index for
202 anthropogenic aerosols over Europe (e.g., Ebert et al., 2002 and 2004; Müller et al., 2002; Mallet et
203 al., 2003 and 2011; Chazette et al., 2005; Raut and Chazette, 2008). For our calculations at 632.8
204 nm we have fixed the imaginary part of the refractive index to 0.01, thus representing a mean
205 absorbing aerosol, and then we have varied the real part between its minimum (1.50) and maximum
206 (1.72) reported value. D_g is then set at the mean ± one standard deviation of the values obtained for
207 the different values of n. We assume in these calculations that the refractive index does not vary
208 with height. After refractive index correction the D_g range for the PCASP becomes 0.10-4.47 µm,
209 with an uncertainty between 1 and 25%. The smallest and the largest size bins of the PCASP, for
210 which the minimum and maximum edges respectively are not defined, have been excluded from the
211 datasets, thus reducing the PCASP D_g range to 0.11-4.17 µm.

212 Once corrected for the refractive index, PCASP data have been combined with those from the CPC
213 to calculate dN_{Aitken}, dN_{Acc}, and dN_{Coarse}. Values for dN_{Acc} and dN_{Coarse} are obtained by integrating
214 the PCASP number concentrations in the 0.1-1.0 µm and 1.0-4.17 µm ranges, while dN_{Aitken} is
215 estimated as the difference between CPC concentration and the integral of PCASP data between 0.1
216 and 3.0 µm. The comparison between the PCASP and the GRIMM below 350 m altitude indicates
217 that the former underestimates by about 50% the aerosol concentration in the range 0.4-1.0 µm (the
218 accuracy of the GRIMM has been verified by optical closure study against simultaneous aircraft
219 nephelometer measurements). This is estimated to induce a ~20% underestimation of the dN_{Acc}
220 calculated here. Conversely, the PCASP underestimation in the 0.4-1.0 µm range has almost a
221 negligible impact on dN_{Aitken}.

CPC measurements, and so dN_{Aitken} data, were not available during SAFMED flights V49, V50, and part of V51.

3.3 Trace gases

Carbon monoxide (CO) and ozone (O_3) mixing ratios were measured by the MOZART instrument described in detail by Nedélec et al. (2003). CO is a long-lived tracer for air masses influenced by combustion processes, whereas O_3 in the troposphere is a photochemical product of the oxidation of CO and volatile organic compounds (VOCs) in the presence of nitrogen oxides (NO_x). CO and O_3 are measured at a resolution of 30 s and 4 s, respectively. The nominal uncertainty is ±5% for CO and ±2% for O_3 (Nedélec et al., 2003). However, a recent airborne intercomparison in May 2014 in the framework of the French ChemCalInt project and the TGOE European Joint Research Activity has suggested a greater uncertainty (up to 30%) on CO measurement by MOZART on-board the ATR-42 (A. Borbon, personal communication, 2015). Trace gas analysis will focus mostly on the vertical distribution of the $\Delta O_3/\Delta CO$ ratio rather than absolute concentrations (see section 5.3) and the uncertainty on CO should not affect data interpretation.

3.4 STP conversion

In order to compare measurements obtained at different altitudes the data presented here are reported at standard temperature and pressure (STP) using T=293.15 K and p=1013.25 hPa (NIST, National Institute of Standards and Technology, values). Hence, the scattering coefficient is scaled to STP conditions and the particle concentrations are given as particles per standard cm^{-3} (scm^{-3}). For a generic parameter x measured at the temperature T and pressure p, the conversion at STP is calculated with the formula:

$$x(STP) = x(T,p)\frac{T}{293.15}\frac{1013.25}{p} \qquad (1).$$

CO and O_3 do not need to be corrected for STP since the mixing ratio does not depend on temperature and pressure.

3.5 Meteorological parameters

The vertical profiles of the pressure (p), the temperature (T), the relative humidity (RH) and the wind components towards the east and the north (U, V) measured on board the ATR-42 have been used to analyse the atmospheric structure during flights. Starting from the measured parameters the potential temperature (θ) has been also calculated as $\theta = T(p_0/p)^{0.286}$ with p_0=1013.2 mbar. For each profile the height of the marine aerosol boundary layer (MABL) and planetary boundary layer (BL) has been estimated visually by looking at the vertical gradients of T, θ, and RH. Meteorological parameters have been also used to calculate the vertical profiles of the gradient Richardson number (Ri):

$$Ri = \frac{g}{\theta}\frac{\partial\theta}{\partial z}\Bigg/\left(\left(\frac{\partial U}{\partial z}\right)^2 + \left(\frac{\partial V}{\partial z}\right)^2\right) \qquad (2).$$

In Eq. (2) g is the gravitational acceleration and z is the height. The Ri number is the ratio between the buoyancy force and the wind shear and it is used to indicate dynamic stability and the formation of clear air turbulence. Turbulence can develop when Ri is below the critical threshold Ri_{crit}=0.25, while it is inhibited for Ri>1 (e.g., Wallace and Hobbs, 2006). In this study the profiles of Ri are used to provide indications of favorable/unfavorable conditions for the development of turbulent conditions within the atmosphere.

3.6 Tracking the air mass back-trajectories

The Lagrangian trajectory model FLEXTRA (FLEXible TRAjectories, Stohl et al., 1995) has been used in selected cases to track the origin of sampled air masses. Five days three-dimensional back-trajectories have been calculated using the ECMWF (European Centre for Medium-Range Weather Forecast) operational analysis with a 0.5° by 0.5° horizontal resolution and up to 30 vertical model levels below 4000 m. The model specific humidity and potential vorticity is also interpolated along the trajectory path.

4. Meteorological conditions, aerosol load, and pollution export regimes

In order to characterize the general aerosol conditions encountered over the Western Mediterranean basin during the TRAQA and the SAFMED campaigns we have plotted the time-series of the aerosol optical depth (τ, ±0.02) at 440 nm and the 440-870 nm Ångström exponent (α) measured with a Cimel sunphotometer (Holben et al., 1998) at the three AERONET stations of Barcelona, Frioul, and Ersa located along the coast around the Western basin (see Fig. 1). Level 1.5 cloud-screened data are used in this study. Data are shown in Fig. 2 and correspond to the period of the campaign of measurements plus 10 days before and after. Table 1 reports the date, location, and main meteorological and export conditions encountered during TRAQA and SAFMED flights.

Over the analysed AERONET sites the aerosol optical depth was below 0.2 before the beginning of the TRAQA campaign and increased, especially at Barcelona and Ersa, to ~0.3-0.5 (with $1<\alpha<2$) in the periods 23-26 June and 3-13 July 2012. Isolated peaks of τ were measured in correspondence of two Saharan dust intrusion events which occurred on the 17-23 June (τ~0.6) and 29 June 2012 (τ~1.4). Different wind regimes occurred during TRAQA and favoured the continental outflow from different regions located around the basin. Two examples of wind maps derived from WRF-Chem model (Grell et al., 2005) at 925 mbar are shown in Fig. 3 for 26 June and 3 July 2012. Main observed meteorological/export conditions can be summarized as follows: (i) on 26-27 June

291 north/north-westerly winds blew across northern Italy determining an air mass outflow towards the
292 Gulf of Genoa (measurements on flights V19-V21); (ii) on the same days a strong Mistral-
293 Tramontane episode (i.e., strong northerly winds developing along the Rhône and Aude valley
294 which bring a northerly/north-westerly flow over the Western Mediterranean, see Fig 3a) favoured
295 the dispersion of pollutants towards the central part of the Western basin. Measurements during the
296 event were performed during flight V20; (iii) on 3-4 July the wind regime was dominated by
297 weasterly/south-weasterly winds mostly blowing at the surface across the Iberian Peninsula and
298 southwestern France (see Fig. 3b). This condition allowed measuring the export of pollution from
299 the Spanish coasts, in particular close to the area of Barcelona (flights V24-V25-V26, see Fig. 1).
300 Additionally, flight V31 sounded the atmospheric structure close to the Spanish coasts reaching the
301 southern urban area of Valencia. The flight was performed one week later (10 July) under a similar
302 meteorological condition characterized by south-westerly winds favouring the export from the
303 Iberian Peninsula towards the basin; (iv) Mistral episodes occurred on the 6-7 and 11 July 2012. In
304 those cases the Mistral wind combined with a persistent westerly flow thus yielding pollution
305 export towards the central and central-eastern part of the Western basin, as measured during flights
306 V27-V28-V30-V32; (v) finally, Saharan dust aerosols were sampled during flights V16 and V20
307 (episode of the 17-23 June) and flights V22 and V23 (episode of the 29 June).

308 During SAFMED the meteorological conditions were more stable and two distinct phases were
309 observed: (i) a stable anticyclone affected the whole Western Mediterranean area during the first
310 half of July until the 26th, thus possibly favouring a more pronounced accumulation of
311 photochemical pollution in this part of the basin. Relatively high values of both τ (~0.2-0.8) and α
312 (~1-2.5) were measured at the three sites of Barcelona, Frioul, and Ersa in this period; (ii) a
313 cyclonic system moving from the Atlantic region towards Europe then affected the Western basin
314 on 28-29 July 2013. Very clean conditions (τ<0.1-0.2) were measured afterwards over the entire
315 region until the end of the SAFMED campaign. Winds were mostly westerly/south-westerly in the

316 first period of the campaign (24-29 July 2013, flights V46, V47, V48, V49, V50), which means that
317 the sampled air flow came mostly from the sea. Then, from 30 July to 1 August 2013 a north-
318 easterly flow affected the SAFMED investigated area thus promoting the export of pollution from
319 Northern Italy towards the Gulf of Genoa (flights V51, V52). A strong Mistral event (29 July-1
320 August) and two Saharan dust outbreaks (27-28 July and 1 August) affected the Western basin,
321 however not influencing the vertical profile observations during SAFMED.

322 In order to identify the distribution of observations during TRAQA and SAFMED as a function of
323 the aerosol type we have plotted in Figure 4 the distribution of the measured scattering coefficient
324 σ_s at 450, 550, and 700 nm as a function of the calculated scattering Ångström exponent α_s for all
325 vertical profiles. The plot shows a similar scattering intensity between cases dominated by coarse
326 particles (α_s<0.5-1.0), such as desert dust, and those dominated by fine particles (α_s> 1.0-1.5), such
327 as pollution aerosols. For both dust and pollution σ_s peaks at about 100-120 Mm^{-1}. The frequency of
328 occurrence of α_s shows that pollution plumes represent the large majority of the cases observed,
329 with more than 70% of measurements with α_s> 1.0.

330

331 **5. Results**

332 Figure 5 shows the box and whisker plots of the aerosol scattering coefficient σ_s at 450, 550, and
333 700 nm, particle number concentration in the Aitken (dN_{Aitken}) and accumulation (dN_{Acc}) diameter
334 ranges, and CO and O_3 measured in the boundary layer (BL) and in the free troposphere (FT) within
335 pollution plumes for all the different vertical soundings analysed in this study. This plot summarizes
336 the range of values observed during TRAQA and SAFMED. On average, the scattering coefficient
337 and CO are larger in the BL compared to the FT, whilst similar ranges of values are measured in the
338 two regions for dN_{Aitken}, dN_{Acc}, and O_3. Even within the single BL and FT the different parameters
339 show a large variability that will be explored in the following paragraphs.

340

5.1 Vertical profiles of aerosol concentration and scattering coefficient

Figure 6 shows the vertical profiles of σ_s, dN_{Acc}, and dN_{Coarse} during TRAQA and SAFMED flights. The date, time and coordinates of each profile, as well as the heights of the top of the marine and planetary boundary layer (MABL and BL) estimated from meteorological data are also indicated in the plot.

For the different vertical soundings the particle concentrations dN_{Acc} and dN_{Coarse} vary in the range ~30-3200 scm^{-3} and ~0.05-40 scm^{-3}, respectively, for plumes with σ_s between 10 and 120 Mm^{-1}. The structure in the scattering profile is generally mirrored in dN_{Acc} profile, and this also reflects the pronounced spectral variability (i.e., decrease for increasing wavelength) of the scattering coefficient, typical of pollution/anthropogenic particles. dN_{Coarse} also contributes to the scattering signal in some cases especially at high altitudes (see V16, V20, V21, V22, and V23 above ~2000 m), and this reflects the low spectral variability of the scattering coefficient. These observations are associated to the dust intrusion episodes which occurred in the Western Mediterranean basin during TRAQA, which however will not be analysed in detail here. Aerosol layers affected by dust have been labelled with a "D" in Fig. 6.

Maxima of the scattering coefficient have been measured for TRAQA flights V21 and V23 (~120 Mm^{-1} for pollution in the BL and ~100 Mm^{-1} in the dust layer), whereas flights V46-V48-V49, during the first and more polluted phase of SAFMED, are the richest in dN_{Acc} (1500-3000 scm^{-3} over the whole column). Minima of σ_s and dN_{Acc} are obtained for flight V51 at the beginning of the second SAFMED phase when clean conditions were observed in the Western Mediterranean.

Pollution plumes observed in the different flights extend from the boundary layer to the free troposphere up to 3000-4000 m altitude. The vertical structure of the aerosol scattering coefficient/particle concentration is linked to the variability of the atmospheric thermodynamic structure and is generally characterized by a first layer confined in the MABL (<400 m, profiles V16, V20, V22, V25, V48, V51), followed by one or more layers within the BL. In the FT pollution

366 particles occur both as single isolated plumes each about 500-1000 m deep (V21, V24, V25, V30,
367 V46, V49), or as a more uniform layer extending from the top of the BL up to 2500-4000 m altitude
368 (V26, V27, V28, V32, V48). The highest values of both the scattering coefficient and dN_{Acc} for
369 pollution are found within the MABL or BL in most cases, while a local minimum of σ_s and dN_{Acc}
370 is generally identified at the top of the BL. The scattering coefficient and the particle concentration
371 measured in the FT are comparable with the values observed in the BL, and in few cases even larger
372 (V25, V26, V30). Only in one case (profile V31) σ_s and dN_{Acc} decrease monotonically with height.
373 The aerosol vertical distribution, both in the BL and in the FT, often presents a strongly stratified
374 structure characterized by the presence of several thin sub-layers within one main identified aerosol
375 plume, as it can be seen in particular in the dN_{Acc} profiles (V20, V21, V22, V25, V46, V49).

376 The particle concentration in the Aitken mode (0.004-0.1 μm; dN_{Aitken}, not shown in Fig. 6) is
377 generally below 5000-6000 scm^{-3} at all altitudes up to 4000 m within pollution plumes. dN_{Aitken} is
378 correlated with dN_{Acc} in most of the observed cases, which indicates the common source of particles
379 in these two size ranges. Few layers exceeding ~10000-15000 scm^{-3} are observed occasionally both
380 in the BL and in the FT. These will be discussed in more detail in Sect. 5.4.

381 The dN_{Acc} and dN_{Aitken} measurements within the BL and in the FT over the sea are comparable with
382 the values measured close to the surface at continental sites under pollution conditions (see Table 2)
383 (Petzold et al., 2002; Mallet et al., 2003 and 2005; Wiegner et al., 2006; Junkermann, 2009;
384 Hamburger et al., 2012; Highwood et al., 2012). This suggests that the export towards the basin
385 favours the redistribution of the pollution plumes along the vertical. Because of mixing in the BL,
386 measured concentrations within the BL can be as high as those observed close to the surface over
387 the continents. Values of dN as high as in the BL are observed in the FT because of transport in
388 specific conditions, as discussed below.

389 The observations of aerosol profiles obtained during TRAQA and SAFMED are representative of
390 the complex transport regimes which characterizes the export towards the Western basin and that is

391 mostly determined by the interaction between regional meteorology and local dynamics (e.g.,
392 Gangoiti et al., 2001). A first example is associated to the measurements in the area of Barcelona.
393 As discussed in Pérez et al. (2004) the presence of mountains up to ~500-3000 m altitude a few
394 kilometres inland favours, during summertime, the recirculation of pollutants along the coasts of
395 Spain. In these cases, the aerosols emitted at the surface in coastal areas are transported inland and
396 uplifted by sea breezes and mountain winds then the plumes are re-injected at different altitudes and
397 distances from the coast. During the TRAQA flights V24, V25, and V26, under the influence of
398 pollution outflow from the Barcelona area, we detected the presence of aerosol layers with elevated
399 concentrations (dN_{Acc}~2000-3000 scm^{-3}) up to 3500 m altitude at a distance of ~30 to 250 km from
400 the coast of Spain. Another example of complex dynamics linked to coastal orography is that
401 associated to the export from northern Italy and the Po Valley towards the Gulf of Genoa. The
402 presence of the Apennine Mountains close to the Ligurian coasts (max elevation ~1500-2000 m)
403 causes the uplift of continental air masses so determining the injection of aerosol plumes at different
404 altitudes both inside and outside the BL. Examples are given by flights V19, V21 and V52 for
405 which pollution aerosols from northern Italy are measured up to ~2000-3000 m altitude throughout
406 the Gulf of Genoa. Finally, another meteorological condition which largely influences the aerosol
407 export and distribution over the Western Mediterranean is the Mistral/Tramontane wind regime.
408 Under the influence of the Mistral flow, atmospheric aerosols can be dispersed as far as hundreds of
409 kilometres over the open sea, as discussed by Salameh et al. (2007). Examples are given in profiles
410 V20 and V28, performed at more than 100 km from the French coasts, for which pollution layers
411 associated to a Mistral flow are measured up to 2000-3000 m altitude.

412

413 **5.2 Trace gases vertical profiles**

414 Figure 7 shows O_3 versus CO for all TRAQA and SAFMED flights, while examples of CO and O_3
415 profiles representatives of different conditions are reported in Fig. 8 and 10.

CO and O_3 vary in the range 60-165 ppbv and 30-85 ppbv, respectively. The 25^{th} and 75^{th} percentiles are 87 and 105 ppbv for CO and 49 and 62 ppbv for O_3, representative of moderate pollution conditions (i.e., Parrish et al., 1998). By comparison, the values measured over land in central Italy during flight V49 are in the range 80-180 ppbv for carbone monoxide and 40-85 ppbv for ozone. CO and O_3 are generally correlated (correlation coefficient R^2~0.5-0.8) within measured pollution plumes, and also correlated with σ_s and N_{Acc} both in the BL and in the FT, which indicates photochemically active plumes. CO is generally higher in the BL, and shows absolute maxima in the lowest levels (V20, V21, V24, V28, V46), then it decreases in the FT. Ozone presents a more complicated vertical structure due to the different photochemical and dynamical processes which control its formation and distribution. At first, local peaks of O_3 correlated with CO are observed in correspondence of pollution plumes both in the BL and in the FT. An absolute maximum of O_3 is sometimes found near the top of the BL (V24, V25, V30) possibly due to aged air masses trapped in the boundary layer. Isolated peaks of O_3 (~75-80 ppbv) not correlated with aerosols and CO are also measured in few cases above 3000-3500 m (V21, V25, V27, V28, V52). The analysis of back-trajectories indicates that these high-altitude ozone layers are associated to the descent of air masses travelling at about 7-8 km, which thus may suggest a downward transport from the upper troposphere or the tropopause region due to a stratosphere-troposphere exchange (Ancellet and Ravetta, 2005). Finally, absolute minima of O_3 (~15-30 ppbv) are measured within the dust layers during flights V20 and V21, maybe related to the dust/ozone heterogeneous reactions which leads to O_3 destruction, as documented in several studies (Bonasoni et al., 2004; Haywood et al., 2011).

5.3 $\Delta O_3/\Delta CO$ and dN_{Aitken}/dN_{Acc} ratios and variability of pollution plume composition

Using the O_3, CO, dN_{Aitken} and dN_{Acc} measurements we have estimated:

- the O_3-CO enhancement ratio ($\Delta O_3/\Delta CO$), i.e. the ratio of the ozone to carbon monoxide variations compared to their baseline values. The $\Delta O_3/\Delta CO$ enhancement ratio is frequently

used to estimate the efficiency of O_3 formation and its export (Parrish et al., 1993; Zhang et al., 2006). From our observations (Fig. 7) we have estimated a background value of ~70 ppbv in the BL and 60 ppbv in the FT for CO and ~30 ppbv for O_3 both in the BL and in the FT.

- The Aitken to accumulation number ratio (dN_{Aitken}/dN_{Acc}), which defines the relative importance of particles in the Aitken and accumulation modes. dN_{Aitken} is generally associated to gas-to-particle conversion and nucleation events and is higher in fresh plumes, while it decreases with the increasing of the plume lifetime due to coagulation or condensation of water-soluble chemical species on the particle surface (Kulmala et al., 2004).

The combination of $\Delta O_3/\Delta CO$ and dN_{Aitken}/dN_{Acc} has been used to retrieve additional information on the atmospheric vertical structure, layering, and particle aging.

Within detected pollution plumes the ΔCO and ΔO_3 reach up to 100-120 ppbv and 45-55 ppbv, respectively, with a corresponding $\Delta O_3/\Delta CO$ ratio which varies in the range ~0.10-2.0 for all cases. The $\Delta O_3/\Delta CO$ ratio is highly noisy and this is due in part to the noise in the CO data, and in part also possibly associated to the slight mismatch between CO and O_3 caused by their different time resolution (30 s for CO and 4 s for O_3). The values of $\Delta O_3/\Delta CO$ obtained in this study are comparable with the range of observations available in the literature for fresh and moderately aged pollution plumes in the BL and in the lower FT (~0.2-1.0) (Chin et al., 1994; Parrish et al., 1998; Zhang et al., 2006; Cristofanelli et al., 2013). dN_{Aitken}/dN_{Acc} is between about 1 and 20 in most of pollution cases, which indicates the presence of both fresh layers rich in Aitken particles and aged plumes poor in Aitken particles. Extremely high values of dN_{Aitken}/dN_{Acc} (~50-200) are measured in few cases in layers with very low dN_{Acc} concentrations.

The large variability in $\Delta O_3/\Delta CO$ and dN_{Aitken}/dN_{Acc} indicates a strong heterogeneity in terms of composition and lifetime for the different observed plumes. This heterogeneity reflects the

complexity in terms of sources, production processes, and transport mechanisms which characterizes the Western basin. In order to illustrate this point, we have selected three examples representative of different conditions observed in different areas of the basin: (i) V19, performed in the Gulf of Genoa in correspondence of continental outflow events from Northern Italy/Po Valley; (ii) V20, performed in Southern France during a Mistral event; (iii) V24, which measured the export of pollution from the area of Barcelona. The vertical profiles of the spectral scattering coefficient σ_s, temperature T, relative humidity RH, dN_{Acc}, dN_{Aitken}, CO, O_3, $\Delta O_3/\Delta CO$, dN_{Aitken}/dN_{Acc} and wind are reported in Fig. 8 for these cases.

1. V19: export from northern Italy/Po Valley. The profile shown for flight V19 (Fig. 8a) is characterized by the presence of three different aerosol structures: the first one below 800 m, characterized by a lower dN_{Aitken}/dN_{Acc} (~1-5) and relatively high $\Delta O_3/\Delta CO$ (~0.4-1.5), possibly associated to moderately aged pollution; the second one between 800 and 2600 m, richer in fine particles (dN_{Aitken}/dN_{Acc}~5-15), so possibly linked to fresher emissions; and the third one above 2600 m, where the ratio dN_{Aitken}/dN_{Acc} rises rapidly, as will be further discussed in Sect. 5.4. The export of fresh pollution at 800-2600 m from northern Italy as observed in V19 may be related to the peculiar orography of this region and the uplift of continental air masses. This is confirmed by the analysis of the back-trajectories (Fig. 9) which indicates that the air masses arriving at 1000 and 2000 m passed over the western Po Valley at an altitude of about 400-1200 m and were then uplifted near the Ligurian coast to enter the basin above the BL. Junkermann (2009) measured high levels of fine particles up to about 2000 m in the western Po Valley, which means that the altitudes of 400-1200 m reached by our investigated air masses could have been sufficient for them to collect fresh emitted particles along their path. Conversely, below 800 m the air mass trajectory shows a longer subsidence over the sea surface in the troposphere which has possibly favoured the advection of more aged plumes, or the mixing with sea salts thus inducing the decrease of the dN_{Aitken}/dN_{Acc} ratio. It should be noted that the aerosol layer in the FT also shows relatively higher values of the

491 $\Delta O_3/\Delta CO$ ratio (~0.6-1.0) compared to the more aged plume in the BL. The enhanced amount of O_3
492 in this air mass can be linked to a high concentration of volatile precursors which may have
493 favoured the build-up of ozone during the plume evolution. In a recent work, Kaiser et al. (2014)
494 suggest that in the Po Valley the high content of formaldehyde, also observed by Junkermann et al.
495 (2009), may be responsible for the excess of O_3 production. Fresh layers in the FT up to ~2000-
496 3000 m possibly associated to pollution export from northern Italy have been also observed during
497 flights V21 and V52 (not shown).

498 *2. V20: export during a Mistral/Tramontane event*. V20 provides an example of export during a
499 Mistral/Tramontane event. As shown in Fig. 8b, winds from the northwest direction are measured at
500 all altitudes during flight V20. The aerosol profile in the BL is characterized in the first ~400 m by
501 the presence of a layer richer in dN_{Aitken} ($dN_{Aitken}/dN_{Acc}>20$) and CO (100 ppbv close to the surface;
502 CO data not available between 150 and 650 m) possibly linked to fresh pollution, followed by the
503 alternation of several layers characterized by a variable dN_{Aitken} (1000-6000 scm^{-3}) and lower CO
504 (~70 ppbv). A local minimum of dN_{Aitken} and σ_s is found at ~400 m. For all these layers the O_3 is
505 very low (~30-40 ppbv) and the $\Delta O_3/\Delta CO$ ratio is <0.6-0.8. At higher altitudes, between 1400 and
506 2000 m, we observe a layer enriched in O_3 ($\Delta O_3/\Delta CO$~1-2) in correspondence of an almost aerosol-
507 free region. This enriched ozone layer might be possibly associated to a downward transport from
508 higher tropospheric layers, as also suggested by the back-trajectories (Fig. 9), as well as to the
509 mixing with ozone rich layers along the air mass trajectory. Larger particles, from long-range
510 transport of Saharan dust at latitudes below 30° N, are measured between 2000 and 3000 m, with a
511 minimum of O_3 (~15-20 ppbv) registered within the layer. Several other flights were performed
512 during Mistral/Tramontane episodes (V27, V28, V30, V32) and show, similarly to V20, the
513 presence of several layers both in the BL and the FT.

514 *3. V24: export from the Barcelona area.* Measurements during V24 may be taken as representative
515 of local recirculation (Pérez et al., 2004). In the V24 profile in Fig. 8c we may recognize up to 5

different aerosol layers. A first layer at <200 m within the MABL, coming from the southwest and directly exported from the area of Barcelona. The layer is characterized by high CO (90-120 ppbv), and relatively low values of dN_{Aitken} (~4000 scm^{-3}) and O_3 (~50 ppbv), which possibly suggest the mixing of pollution with marine particles close to the sea surface. A second layer of fresher particles, always coming from the southwestern direction, is observed above the MABL between 200 and 600 m (dN_{Aitken}~6000-8000 scm^{-3}, O_3~70 ppb, with dN_{Aitken}/dN_{Acc}~5-15, and $\Delta O_3/\Delta CO$~0.8-1.5). A third, more aged, sublayer (dN_{Aitken}/dN_{Acc}~2-5, $\Delta O_3/\Delta CO$~0.8-1.0) is observed within the BL between 600 and 1000 m. The FT is characterized by the presence of moderately aged plumes from ~1000 to 2800 m (dN_{Aitken}/dN_{Acc}~2-10, $\Delta O_3/\Delta CO$~0.2-0.8), and a very aged plume at 2800-3800 m almost deprived in Aitken particles and richer in O_3 (dN_{Aitken}/dN_{Acc}<1, $\Delta O_3/\Delta CO$~0.6-1.5). A marked local minimum is observed at the top of the BL for σ_s, dN_{Acc}, dN_{Aitken}, CO, and O_3, suggesting the presence of air masses with different origin between the BL and the FT. This is also confirmed by the analysis of the back-trajectories (Fig. 9) which indicates a low level air masses coming from the Spanish coasts in the BL, and air masses travelling at higher altitudes in the FT. In particular, the layer at 2800-3800 m is possibly associated to an intercontinental transport from Northern America, as shown in the trajectory ending at 3500 m. A similar structure characterized by the alternation of fresher and more aged plumes in the BL and FT is also observed in V25 for which aerosol layers are detected up to 4000 m altitude.

The detailed analysis of these three events evidences the complexity of the atmospheric structure over the Western Mediterranean basin in link with the different dynamical processes involved.

5.4 Layers with enhanced Aitken mode particle numbers

Isolated layers with dN_{Aitken}~10000-15000 scm^{-3} have been observed occasionally both in the BL and in the FT. The vertical profiles of dN_{Aitken} for some selected cases are shown in Fig. 10.

For about half of the observed events the dN_{Aitken} layer appears related to a simultaneous increase in dN_{Acc}, CO, and O_3, which suggests that the layer has been transported from a region directly emitting in this size range. These cases are: V16 at ~200-400 m, V21 at ~400-800 m, V28 at ~250 m, and V31 at ~1000-3000 m (only V28 and V31 are shown in Fig. 10). The most remarkable example is V31 (Fig. 10a), performed close to the coasts of Spain near Valencia, for which the high dN_{Aitken} layer extends from the top of the BL to ~3000 m altitude. The wind vector and the back-trajectories (not shown) indicates that the air mass comes from the western-southwestern direction above 1000 m, so the dN_{Aitken} layer can be directly related to pollution export from the urban region of Valencia.

In all the other cases the high dN_{Aitken} layer is generally not related to simultaneous dN_{Acc} and O_3 increase. Two of these cases (V16 at ~800-1000 m and V28 at ~100 m) occur in the BL.

For the V28 layer (Fig. 10b) the dN_{Aitken} is correlated with CO which might indicate the influence of local emissions close to the surface level (i.e., ship emissions). CO values are relatively high (140-160 ppbv) within the layer. It has been often assumed that new particle formation events (NPF) only occur in almost clean environments (e.g., O'Dowd et al., 2010; Sellegri et al., 2010), and that they are suppressed under polluted conditions. In a recent study, Brines et al. (2014) show the occurrence of NPF events also in urban areas with high level of pollution in the Mediterranean region. So, we explore the possibility of NPF in our observations. Given the size ranges of the CPC and PCASP, however, we cannot discriminate within dN_{Aitken} the particle concentration in the sole 4-20 nm range, i.e. the size range involved in nucleation. So it is not possible to directly associate the V28 observations to NPF. In order to obtain a qualitative indication of the possible occurrence of NPF, we have looked at the air mass dynamics within the layer. Several studies suggest, in fact, that NPF might be favoured by turbulence and air mass mixing (e.g., Nilsson et al., 2001; Wehner et al., 2010). We have thus looked at the gradient Richardson number (Ri) which gives information on the atmospheric dynamical stability. Vertical profiles of Ri are also shown in Fig. 10. For V28 the

565 vertical profile of Ri indicates that below 200 m the Ri number is consistently below zero, which
566 suggests well established turbulent conditions possibly favouring NPF in this layer.

567 In other two cases (V19, Fig. 10c, and V26, Fig. 10d), under lower pollution conditions (CO < 100),
568 we measured high dN_{Aitken} concentration in correspondence of low dN_{Acc} layers in the FT at ~2800-
569 3000 m for V19 and 3500-4500 m for V26. For V19 and V26 layers, dN_{Aitken} seems anticorrelated
570 to CO. Also in this case the Richardson number is below Ri_{crit} in correspondence of the Aitken peak
571 meaning that conditions are favorable for turbulence within the layer, and this may indicate also in
572 this case the possible role of NPF.

573 Finally, a case of high dN_{Aitken} concentration has been also observed in correspondence of dust
574 particles between ~3000 and 4000 m (V23b, Fig. 10e). This layer can be possibly linked to the
575 photochemically-induced nucleation which may occur in presence of dust and SO_2 as hypothesised
576 in a recent study by Dupart et al. (2012) and observed by Nie et al. (2014).

577

578 **6. Conclusions**

579 The data presented in this paper gives an overview of the distribution of aerosols and trace gases
580 within the tropospheric column up to 5000 m above the Western Mediterranean basin.

581 These data add to the very few available measurements of aerosol and trace gases vertical profiles
582 over the sea surface in the Central (e.g., Junkermann, 2001; Meloni et al., 2003; Di Iorio et al.,
583 2003; Pace et al., 2014) and Eastern (e.g., Formenti et al., 2002; Dulac and Chazette, 2003) parts of
584 the basin thus contributing to improve the description of the atmospheric composition and structure
585 over the whole Mediterranean area.

586 Observations from the present study indicate that continental pollution strongly affects the
587 composition and structure of the Western Mediterranean basin both close to coastal regions and in
588 the open sea. Pollution layers extend up to 250 km far from the coasts and reach up to 3000-4000 m

589 altitude, presenting a complex and highly stratified structure. The measured particle concentration is
590 comparable with the values reported for continental Europe (Petzold et al., 2002; Junkermann,
591 2009; Hamburger et al., 2012).

592 Pollution plumes with different compositions, origins, and lifetimes are observed in link with the
593 different observed dynamical export conditions and meteorological regimes. The aerosol and trace
594 gas observations during TRAQA and SAFMED are consistent with the results of former campaigns
595 and with the interpretation of observed or well known air-masses dynamics and meteorological
596 phenomena that can occur in the Western basin (Flamant and Pelon, 1996; Millan et al., 1997;
597 Gangoiti et al., 2001; Pérez et al., 2004; Mallet et al., 2005).

598 The large heterogeneity in aerosol compositions, origins, and lifetimes as documented in this study
599 can reflect in a large heterogeneity of aerosol optical properties, with consequences for their direct
600 radiative effect in this part of the basin. This aspect will be investigated in a companion paper
601 analysing the TRAQA and SAFMED in situ measurements of the aerosol absorption and scattering
602 properties and their variability.

603 From the present observations, it is also interesting to note the relatively high values of dN_{Aitken}
604 measured both in the BL and the FT, which evidences the important contribution of ultrafine
605 particles at all altitudes over the basin. These can be linked to the different export mechanisms
606 previously discussed, as well as the possible occurrence of NPF events. Aitken particle profiles are
607 very rare over the sea surface in the Mediterranean (e.g., Junkermann et al. 2001; Pace et al., 2015)
608 and data comparison is quite difficult. Few studies have observed NPF in the FT in continental
609 areas (Boulon et al., 2010; Rose et al., 2014) and suggest that the export of pollution into the upper
610 troposphere, as it is common in the Western basin, might promote the occurrence of these events.
611 The observations of the present study may thus also have very large implications due to the crucial
612 role of NPF in controlling the atmospheric cloud condensation nuclei concentration (Spracklen et
613 al., 2008) and the associated aerosol indirect effect on climate.

Author contributions

J.-L.A., F.R., G.A., M.B., A.B., P.F. and K.S. designed the TRAQA and SAFMED experiments and coordinated the campaigns. C.G., N.G., and C.D.B operated the instruments on board the ATR-42 during the flights. C.D.B. performed the data analysis with contributions from L.D., P.F., F.R., A.B., G.A., J.-C.R., and M.B.. G.A. performed the FLEXTRA simulations. J.-C.R. performed the WRF-Chem simulations. C.D.B. wrote the manuscript.

Acknowledgements

All measurement presented here are from the Chemistry-Aerosol Mediterranean Experiment project (ChArMEx, http://charmex.lsce.ipsl.fr), which is the atmospheric component of the French multidisplinary program MISTRALS (Mediterranean Integrated Studies aT Regional And Local Scales). ChArMEx-France was principally funded by INSU, ADEME, ANR, CNES, CTC (Corsica region), EU/FEDER, Météo-France, and CEA. TRAQA was funded by ADEME/PRIMEQUAL and MISTRALS/ChArMEx programmes and Observatoire Midi-Pyrénées. SAFMED was funded by the ANR project SAF-MED (Secondary Aerosol Formation in the MEDiterranean, grant SIMI6 ANR-12-BS06-0013). C. Di Biagio thanks the Centre National des Etudes Spatiales (CNES) for financial support.

The authors wish to thank the technicians, pilots and ground crew of SAFIRE (Service des Avions Francais Instruments pour la Recherche en Environnement) for facilitating the instrument integration and conducting flying operations. We thank S. Chevaillier, L. Girault, R. Loisil, J. Pelon, S. Triquet, and P. Zapf for their contribution during the campaigns. We thank S. Basart, J. M. Baldasano, M. Mallet, P. Goloub, J. Piazzola and their staff for establishing and maintaining the Barcelona, Ersa, and Frioul AERONET sites. Helpful discussions with G. Pace are gratefully

638 acknowledged. We thank also two anonymous reviewers whose suggestions helped to clarify the
639 manuscript.

640

641

642 **References**

643 Ancellet, G. and Ravetta, F.: Analysis and validation of ozone variability observed by lidar during
644 the ESCOMPTE-2001 campaign, Atmos. Res., 74, 435–459, 2005.

645 Anderson, T. L., Covert, D. S., Marshall, S. F., Laucks, M. L., Charlson, R. J., Waggoner, A. P.,
646 Ogren, J. A., Caldow, R., Holm, R. L., Quant, F. R., Sem, G. J., Wiedensholer, A., Ahlquist, N.
647 A., and Bates, T. S.: Performance characteristics of a high-sensitivity, three-wavelength, total
648 scatter/backscatter nephelometer, J. Atmos. Ocean. Tech., 13, 967–986, 1996.

649 Anderson, T. L. and Ogren, J. A.: Determining aerosol radiative properties using the TSI 3563
650 integrating nephelometer, Aerosol Sci. Technol., 29, 57–69, 1998.

651 Bonasoni, P., Cristofanelli, P., Calzolari, F., Bonafè, U., Evangelisti, F., Stohl, A., Zauli Sajani, S.,
652 van Dingenen, R., Colombo, T., and Balkanski, Y.: Aerosol-ozone correlations during dust
653 transport episodes, Atmos. Chem. Phys., 4, 1201-1215, doi:10.5194/acp-4-1201-2004, 2004.

654 Boucher, O., Randall, D., Artaxo, P., Bretherton, C., Feingold, G., Forster, P., Kerminen, V.-M.,
655 Kondo, Y., Liao, H., Lohmann, U., Rasch, P., Satheesh, S. K., Sherwood, S., Stevens, B., and
656 Zhang, X. Y.: Clouds and Aerosols. In:Climate Change 2013: The Physical Science Basis.
657 Contribution of Working Group I to the Fifth Assessment Report of the Intergovernmental Panel
658 on Climate Change [Stocker, T.F., D. Qin, G.-K. Plattner, M. Tignor, S.K. Allen, J. Boschung,
659 A. Nauels, Y. Xia, V. Bex and P.M. Midgley (eds.)]. Cambridge University Press, Cambridge,
660 United Kingdom and New York, NY, USA, 571-657, 2013.

661 Boulon, J., Sellegri, K., Venzac, H., Picard, D., Weingartner, E., Wehrle, G., Collaud Coen, M.,
662 Bütikofer, R., Flückiger, E., Baltensperger, U., and Laj, P.: New particle formation and ultrafine
663 charged aerosol climatology at a high altitude site in the Alps (Jungfraujoch, 3580 m a.s.l.,
664 Switzerland), Atmos. Chem. Phys., 10, 9333–9349, doi: 10.5194/acp-10-9333-2010, 2010.

665 Brines, M., Dall'Osto, M., Beddows, D. C. S., Harrison, R. M., Gómez-Moreno, F., Núñez, L.,
666 Artíñano, B., Costabile, F., Gobbi, G. P., Salimi, F., Morawska, L., Sioutas, C., and Querol, X.:
667 Frequency of new particle formation events in the urban Mediterranean climate, Atmos. Chem.
668 Phys. Discuss., 14, 26463-26494, doi:10.5194/acpd-14-26463-2014, 2014.

669 Chazette, P., Randriamiarisoa, H., Sanak, J., Couvert, P., and Flamant, C.: Optical properties of
670 urban aerosol from airborne and ground based in situ measurements performed during the
671 ESQUIF program, J. Geophys. Res., 110, D02206, doi:10.1029/2004JD004810, 2005.

672 Chin, M., Jacob, D. J., Munger, J. W., Parrish, D. D., and Doddridge, B. G.: Relationship of ozone
673 and carbon monoxide over North America, J. Geophys. Res., 99, 14,565–14,573, 1994.

674 Colette, A., Ancellet, G., Menut, L., and Arnold, S. R.: A Lagrangian analysis of the impact of
675 transport and transformation on the ozone stratification observed in the free troposphere during
676 the ESCOMPTE campaign, Atmos. Chem. Phys., 6, 3487-3503, doi:10.5194/acp-6-3487-2006,
677 2006.

678 Cristofanelli, P., Fierli, F., Marinoni, A., Calzolari, F., Duchi, R., Burkhart, J., Stohl, A., Maione,
679 M., Arduini, J., and Bonasoni, P.: Influence of biomass burning and anthropogenic emissions on
680 ozone, carbon monoxide and black carbon at the Mt. Cimone GAW-WMO global station (Italy,
681 2165 m a.s.l.), Atmos. Chem. Phys., 13, 15–30, 2013.

682 Di Iorio, T., di Sarra, A., Junkermann, W., Cacciani, M., Fiocco, G., and Fua`, D.: Tropospheric
683 aerosols in the Mediterranean: 1. Microphysical and optical properties, J. Geophys. Res.,
684 108(D10), 4316, doi:10.1029/2002JD002815, 2003.

685 Drobinski, P, Saïd, F., Ancellet, G., Arteta, J. Augustin, P., Bastin, S., Brut, A., Caccia, J. L.,
686 Campistron, B., Cautenet, S., Colette, A., Coll, I., Corsmeier, U., Cros, B., Dabas, A., Delbarre,
687 H., Dufour, A., Durand, P., Guénard, V., Hasel, M., Kalthoff, N., Kottmeier, C., Lasry, F.,
688 Lemonsu, A., Lohou, F., Masson, V., Menut, L., Moppert, C., Peuch, V. H., Puygrenier, V.,
689 Reitebuch, O., and Vautard, R.: Regional transport and dilution during high-pollution episodes in
690 southern France: Summary of findings from the Field Experiment to Constraint Models of
691 Atmospheric Pollution and Emissions Transport (ESCOMPTE), J. Geophys. Res., 112, D13105,
692 doi:10.1029/2006JD007494, 2007.

693 Dulac, F., and Chazette, P.: Airborne study of a multi-layer aerosol structure in the eastern
694 Mediterranean observed with the airborne polarized lidar ALEX during a STAAARTE campaign
695 (7 June 1997), Atmos. Chem. Phys., 3, 1817-1831, doi:10.5194/acp-3-1817-2003, 2003.

696 Dupart, Y.; King, S. M., Nekat, B., Nowak, A., Wiedensohler, A., Herrmann, H., David, G.,
697 Thomas, B., Miffre, A., Rairoux, P., D'Anna, B., and George, C.: Mineral dust photochemistry
698 induces nucleation events in the presence of SO_2. PNAS, 109, (51), 20842–20847, 2012.

699 Ebert, M., Weinbruch, S., Rausch, A., Gorzawski, G., Hoffmann, P., Wex, H., and Helas, G.: The
700 complex refractive index of aerosols during LACE 98 as derived from the analysis of individual
701 particles, J. Geophys. Res., 107, D21, 8121, doi:10.1029/2000JD000195, 2002.

702 Ebert, M., Weinbruch, S., Hoffmann, P., and Ortner, H. M.: The chemical composition and complex
703 refractive index of rural and urban influenced aerosols determined by individual particle
704 analysis, Atmos. Environ., 38, 6531–6545, 2004.

705 Flamant, C., and Pelon, J.: Atmospheric boundary-layer structure over the Mediterranean during a
706 Tramontane event, Quart. J. Roy. Meteorol. Soc., 122, 1741–1778, 1996.

707 Formenti, P., Reiner, T., Sprung, D., Andreae, M. O., Wendisch, M., Wex, H., Kindred, D., Dewey,
708 K., Kent, J., Tzortziou, M., Vasaras, A., and Zerefos, C.: STAAARTE-MED 1998 summer
709 airborne measurements over the Aegean Sea, 1, Aerosol particles and trace gases, J. Geophys.
710 Res., 107, D21, doi:10.1029/2001JD001337, 2002.

711 Formenti, P., Rajot, J. L., Desboeufs, K., Saïd, F., Grand, N., Chevaillier, S., and Schmechtig, C.:
712 Airborne observations of mineral dust over western Africa in the summer Monsoon season:
713 spatial and vertical variability of physico-chemical and optical properties, Atmos. Chem. Phys.,
714 11, 6387-6410, doi:10.5194/acp-11-6387-2011, 2011.

715 Gangoiti, G., M. M. Millán, R. Salvador, E. Mantilla: Long-Range transport and recirculation of
716 pollutants in the Western Mediterranean during the RECAPMA Project. Atmos. Environ., 35,
717 6267-6276, 2001.

718 Gkikas, A., Houssos, E. E., Hatzianastassiou, N., Papadimas, C. D., and Bartzokas, A.: Synoptic
719 conditions favouring the occurrence of aerosol episodes over the broader Mediterranean basin,
720 Q. J. R. Meteorol. Soc., 138: 932–949. doi:10.1002/qj.978, 2012.

721 Grell, G. A., Peckham, S. E., Schmitz, R., McKeen, S. A., Frost, G., Skamarock, W. C., and Eder,
722 B.: Fully coupled “online” chemistry within the WRF model, Atmos. Environ., 39, 6957–6975,
723 2005.

724 Hamburger, T., McMeeking, G., Minikin, A., Petzold, A., Coe, H., and Krejci, R.: Airborne
725 observations of aerosol microphysical properties and particle ageing processes in the troposphere
726 above Europe, Atmos. Chem. Phys., 12, 11533-11554, doi:10.5194/acp-12-11533-2012, 2012.

727 Haywood, J., Johnson, B., Osborne, S., Mulcahy, J., Brooks, M., Harrison, M., Milton, S., and
728 Brindley, H.: Observations and modelling of the solar and terrestrial radiative effects of Saharan
729 dust: a radiative closure case-study over oceans during the GERBILS campaign, Q. J. R.
730 Meteorol. Soc., 137, 1211–1226, doi:10.1002/qj.770, 2011.

731 Highwood, E. J., Northway, M. J., McMeeking, G. R., Morgan, W. T., Liu, D., Osborne, S.,
732 Bower, K., Coe, H., Ryder, C., and Williams, P.: Aerosol scattering and absorption during the
733 EUCAARI-LONGREX flights of the Facility for Airborne Atmospheric Measurements (FAAM)
734 BAe-146: can measurements and models agree?, Atmos. Chem. Phys., 12, 7251-7267,
735 doi:10.5194/acp-12-7251-2012, 2012.

736 Holben, B. N., Eck, T. F, Slutsker, I., Tanré, D., Buis, J. P., Setzer, A., Vermote, E., Reagan, J. A.,
737 Kaufman, Y., Nakajima, T., Lavenu, F., Jankowiak, I., and Smirnov, A.: AERONET: a federated
738 instrument network and data archive for aerosol characterization, Rem. Sens. Environ., 66, 1–16,
739 1998.

740 Jiménez, P., Pérez, C., Rodriguez, A., and Baldasano, J. M. : Correlated levels of particulate matter
741 and ozone in the western Mediterranean basin: Air quality and lidar measurements, 22nd Annual
742 Conference Am. Assoc. for Aerosol Res., Anaheim, California, 20-24 October 20-24 2003,
743 2003.

744 Jiménez, P., Lelieveld, J., and Baldasano, J. M.: Multiscale modeling of air pollutants dynamics in
745 the northwestern Mediterranean basin during a typical summertime episode, J. Geophys. Res.,
746 111, D18306, doi:10.1029/2005JD006516, 2006.

747 Jiménez-Guerrero, P., Jorba, O., Baldasano, J. M., and Gassó, S.: The use of a modelling system as
748 a tool for air quality management: Annual high-resolution simulations and evaluation, Sci. Tot.
749 Environ., 390, 323–340, 2008.

750 Junkermann, W.: An ultralight aircraft as platform for research in the lower troposphere: System
751 performance and first results from radiation transfer studies in stratiform aerosol layers and
752 broken cloud conditions, J. Atmos. Oceanic Technol., 18, 934–946, 2001.

753 Junkermann, W.: On the distribution of formaldehyde in the western Po-Valley, Italy, during 800
754 FORMAT 2002/2003, Atmos. Chem. Phys., 9, 9187-9196, doi:10.5194/acp-9-9187-2009, 2009.

755 Kaiser, J., Wolfe, G. M., Bohn, B., Broch, S., Fuchs, H., Ganzeveld, L. N., Gomm, S., Häseler, R.,
756 Hofzumahaus, A., Holland, F., Jäger, J., Li, X., Lohse, I., Lu, K., Rohrer, F., Wegener, R.,
757 Mentel, T. F., Kiendler-Scharr, A., Wahner, A., and Keutsch, F. N.: Evidence for an unidentified
758 ground-level source of formaldehyde in the Po Valley with potential implications for ozone
759 production, Atmos. Chem. Phys. Discuss., 14, 25139-25165, doi:10.5194/acpd-14-25139-2014,
760 2014.

761 Kallos, G., Astitha, M., Katsafados, P., and Spyrou, C.: Long-range transport of anthropogenically
762 and naturally produced particulate matter in the Mediterranean and North Atlantic: Current state
763 of knowledge, J. Appl. Meteorol. Climatol., 46, 1230–1251, 2007.

764 Kulmala, M., Vehkamaki, H., Petaja, T., Dal Maso, M., Lauri, A., Kerminen, V.-M., Birmili, W.,
765 and McMurry, P.H.: Formation and growth rates of ultrafine atmospheric particles: A review of
766 observations, J. Aerosol Sci., 35(2), 143–176, 2004.

767 Lelieveld, J., Berresheim, H., Borrmann, S., Crutzen, P. J., Dentener, F. J., Fischer, H., Feichter, J.,
768 Flatau, P. J., Heland, J., Holzinger, R., Korrmann, R., Lawrence, M. G., Levin, Z., Markowicz,
769 K. M., Mihalopoulos, N.; Minikin, A., Ramanathan, V., de Reus, M., Roelofs, G. J., Scheeren,

H. A., Sciare, J., Schlager, H., Schultz, M., Siegmund, P., Steil, B., Stephanou, E. G., Stier, P., Traub, M., Warneke, C., Williams, J., and Ziereis H.: Global air pollution crossroads over the Mediterranean, Science, 298, 794–799, doi:10.1126/science.1075457, 2002.

Liu, Y. and Daum, P.: The effect of refractive index on size distributions and light scattering coefficients derived from optical particle counters, J. Aerosol Sci., 31, 945–957, 2000.

Mallet, M., Roger, J. C., Despiau, S., Dubovik, O., and Putaud, J. P.: Microphysical and optical properties of aerosol particles in urban zone during ESCOMPTE, Atmos. Res., 69, 73–97, 15 2003.

Mallet, M., Van Dingenen, R., Roger, J. C., Despiau, S., and Cachier, H.: In situ airborne measurements of aerosol optical properties during photochemical pollution events, J. Geophys. Res., 110, D03205, doi:10.1029/2004JD005139, 2005.

Mallet, M., Gomes, L., Solmon, F., Sellegri, K., Pont, V., Roger, J. C., Missamou, T., and Piazzola, J.: Calculation of key optical properties of the main anthropogenic aerosols over the Western French coastal Mediterranean Sea, Atmos. Res., 101, 396–411, 2011.

Meloni, D., di Sarra, A., DeLuisi, J., Di Iorio, T., Fiocco, G., Junkermann, W., and Pace, G.: Tropospheric aerosols in the Mediterranean: 2. Radiative effects through model simulations and measurements, J. Geophys. Res., 108(D10), 4317, doi:10.1029/2002JD002807, 2003.

Millán, M., Salvador, R., Mantilla, E., and Artinãno, B.: Meteorology and photochemical air pollution in Southern Europe: experimental results from EC research projects, Atmos. Environ., 30 (12), 1909–1924, 1996.

Millan, M. M., Salvador, R., Mantilla, E., and Kallos, G.: Photooxidant dynamics in the Western Mediterranean in summer: Results from European research projects, J. Geophys. Res., 102(D7), 8811–8823, 1997.

Millán, M. M., Mantilla, E., Salvador, R., Carratala, A., Sanz, M. J., Alonso, L., Gangoiti, G., and Navazo, M.: Ozone cycles in the western Mediterranean basin: interpretation of monitoring data in complex terrain, J. Appl. Meteorol., 4, 487–507, 2000.

Monks, P., Granier, C., Fuzzi, S., Stohl, A., Williams, M., Akimoto, H., Amann, M., Baklanov, A., Baltensperger, U., Bey, I., Blake, N., Blake, R., Carslaw, K., Cooper, O., Dentener, F., Fowler, D., Fragkou, E., Frost, G., Generoso, S., Ginoux, P., Grewe, V., Guenther, A., Hansson, H., Henne, S., Hjorth, J., Hofzumahaus, A., Huntrieser, H., Isaksen, I., Jenkin, M., Kaiser, J., Kanakidou, M., Klimont, Z., Kulmala, M., Laj, P., Lawrence, M., Lee, J., Liousse, C., Maione, M., McFiggans, G., Metzger, A., Mieville, A., Moussiopoulos, N., Orlando, J., O'Dowd, C., Palmer, P., Parrish, D., Petzold, A., Platt, U., Pöschl, U., Prévôt, A., Reeves, C., Reimann, S., Rudich, Y., Sellegri, K., Steinbrecher, R., Simpson, D., ten Brink, H., Theloke, J., van der Werf, G., Vautard, R., Vestreng, V., Vlachokostas, C., and von Glasow, R.: Atmospheric composition change – global and regional air quality, Atmos. Environ., 43, 5268–5350, doi:10.1016/j.atmosenv.2009.08.021, 2009.

Müller, D., Ansmann, A., Wagner, F., Franke, K., and Althausen, D.: European pollution outbreaks during ACE 2: Microphysical particle properties and single-scattering albedo inferred from multiwavelength lidar observations, J. Geophys. Res., 107, D15, 4248, 10.1029/2001JD001110, 2002.

Nedélec, P., Cammas, J.-P., Thouret, V., Athier, G., Cousin, J.-M., Legrand, C., Abonnel, C., Lecoeur, F., Cayez, G., and Marizy, C.: An improved infrared carbon monoxide analyser for routine measurements aboard commercial Airbus aircraft: technical validation and first scientific results of the MOZAIC III programme, Atmos. Chem. Phys., 3, 1551–1564, doi:10.5194/acp-3-1551-2003, 2003.

Nie, W., Ding, A., Wang, T., Kerminen, V.-M., George, C., Xue, L., Wang, W., Zhang, Q., Petaja, T., Qi, X., Gao, X., Wang, X., Yang, X., Fu, C., and Kulmala, M.: Polluted dust promotes new particle formation and growth, Sci. Rep., 4, 6634, doi:10.1038/srep06634, 2014.

Nilsson, E. D., Rannik, U., Kulmala, M., Buzorius, G., and, O'Dowd, C. D.: Effects of continental boundary layer evolution, convection, turbulence and entrainment, on aerosol formation, TellusB, 53, 441–461, 2001.

O'Dowd, C., Monahan, C., and Dall'Osto, M.: On the occurrence of open ocean particle production and growth events, Geophys. Res. Lett., 37, L19805, doi:10.1029/2010GL044679, 2010.

Pace, G., di Sarra, A., Meloni, D., Piacentino, S., and Chamard, P.: Aerosol optical properties at Lampedusa (Central Mediterranean). 1. Influence of transport and identification of different aerosol types, Atmos. Chem. Phys., 6, 697-713, doi:10.5194/acp-6-697-2006.

Pace, G., Junkermann, W., Vitali, L., di Sarra, A., Meloni, D., Cacciani, M., Cremona, G., Iannarelli, A. M., and Zanini, G: On the complexity of the boundary layer structure and aerosol vertical distribution in the coastal Mediterranean regions: a sea breeze, desert dust transport, and free-tropospheric air intrusion case study in Southern, submitted to TellusB, 2015.

Parrish, D. D., Holloway, J. S., Trainer, M., Murphy, P. C., Fehsenfeld, F. C., and Forbes, G. L.: Export of North America ozone pollution to the North Atlantic Ocean, Science, 259, 1436–1439, 1993.

Parrish, D. D., Trainer, M., Holloway, J. S., Yee, J. E., Warshawsky, M. S., Fehsenfeld, F. C., Forbes, G. L., and Moody, J. L.: Relationships between ozone and carbon monoxide at surface sites in the North Atlantic region, J. Geophys. Res., 103, 13,357– 13,376, 1998.

Pérez, C., Sicard, M., Jorba, O., Comeron, A., and Baldasano, J. M.: Summertime re-recirculations of air pollutants over the North-Eastern Iberian coast observed from systematic EARLINET lidar measurements in Barcelona, Atmos. Environ., 38, 3983–4000, 2004.

Pérez, N., Pey, J., Castillo, S., Viana, M., Alastuey, A., and Querol, X.: Interpretation of the variability of levels of regional background aerosols in the Western Mediterranean, Sci. Tot. Environ., 407, 527–540, 2008.

Petzold, A., Fiebig, M., Flentje, H., Keil, A., Leiterer, U., Schroder, F., Stifter, A., Wendisch, M., and Wendling, P.: Vertical variability of aerosol properties observed at a continental site during the Lindenberg Aerosol Characterization Experiment (LACE 98), J. Geophys. Res., 107, 8128, doi:10.1029/2001JD001043, 2002.

Pey, J., Querol, X., and Alastuey, A.: Discriminating the regional and urban contributions in the North-Western Mediterranean: PM levels and composition, Atmos Environ, 44, 1587–96, 2010.

Raut, J.-C., and Chazette, P.: Vertical profiles of urban aerosol complex refractive index in the frame of ESQUIF airborne measurements, Atmos. Chem. Phys., 8, 901–919, 2008.

Rose,C., Sellegri, K., Asmi, E., Hervo, M., Freney, E., Junninen, H., Duplissy, J., Sipilä, M., Kontkanen, J., Lehtipalo, K., and Kulmala, M.: Major contribution of neutral clusters to new particle formation in the free troposphere, Atmos. Chem. Phys. Discuss., 14, 18355–18388, 2014.

Salameh, T., Drobinski, P., Menut, L., Bessagnet, B., Flamant, C., Hodzic, A., and Vautard, R.: Aerosol distribution over the western Mediterranean basin during a Tramontane/Mistral event, Ann. Geophys., 25, 2271–2291, 2007.

Sellegri, K., Laj, P., Venzac, H., Boulon, J., Picard, D., Villani, P., Bonasoni, P., Marinoni, A., Cristofanelli, P., and Vuillermoz, E.: Seasonal variations of aerosol size distributions based on long-term measurements at the high altitude Himalayan site of Nepal Climate Observatory-

Pyramid (5079 m), Nepal, Atmos. Chem. Phys., 10, 10679–10690, doi:10.5194/acp-10-10679-2010, 2010.

Soriano, C., Baldasano, J. M., Buttler, W. T., and Moore, K.: Circulatory patterns of air pollutants within the Barcelona air basin in a summertime situation: lidar and numerical approaches. Bound.-Lay. Meteorol., 98 (1), 33–55, 2001.

Spracklen, D. V., Carslaw, K. S., Kulmala, M., Kerminen, V.-M., Sihto, S.-L., Riipinen, I., Merikanto, J., Mann, G. W., Chipperfield, M. P., and Wiedensohler, A.: Contribution of particle formation to global cloud condensation nuclei concentrations, Geophys. Res. Lett., 35, *L06808*, doi:10.1029/2007GL033038, 2008.

Stohl, A., Wotawa, G., Seibert, P., and Krompkolb, H.: Interpolation errors in wind fields as a function of spatial and temporal resoloution and their impact on different types of kinematic trajectories, J. Appl. Meteorol., 34, 2149–2165, 1995.

Velchev, K., Cavalli, F., Hjorth, J., Marmer, E., Vignati, E., Dentener, F., and Raes, F.: Ozone over the Western Mediterranean Sea – results from two years of shipborne measurements, Atmos. Chem. Phys., 11, 675-688, doi:10.5194/acp-11-675-2011, 2011.

Wallace J.M., and Hobbs, P.V.: Atmospheric science: an introductory survey (2nd edition). International Geophysics Series 92, Academic press, Burlington, 484pp, 2006.

Wehner, B., H. Siebert, A. Ansmann, F. Ditas, P. Seifert, F. Stratmann, A. Wiedensohler, A. 956 Apituley, R. A. Shaw, H. E. Manninen, and M. Kulmala (2010), Observations of turbulence induced new particle formation in the residual layer, Atmos. Chem. Phys., 10, 4319–4330, 958 doi:10.5194/acp-10-4319-2010.

Wiegner, M., Emeis, S., Freudenthaler, V., Heese, B., Junkermann, W., Münkel, C., Schäfer, K., Seefeldner, M., and Vogt, S.: Mixing layer height over Munich, Germany: variability and comparisons of different methodologies, J. Geophys. Res., 111, D13201, doi:10.1029/2005JD006593, 2006.

Zhang, L., Jacob, D. J., Bowman, K. W., Logan, J. A., Turquety, S., Hudman, R. C., Li, Q., Beer, R., Worden, H. M., Worden, J. R., Rinsland, C. P., Kulawik, S. S., Lampel, M. C., Shephard, M. W., Fisher, B. M., Eldering, A., and Avery M. A.: Ozone-CO correlations determined by the TES satellite instrument in continental outflow regions, Geophys. Res. Lett., 33, L18804, doi:10.1029/2006GL026399, 2006.

Tables

Table 1. Summary of information on the TRAQA and SAFMED flights.

Measurement campaign	Flight number	Date	Take off-landing time (UTC)	Departure-arrival	Geographic area investigated	Description
TRAQA 2012	V16	20/06/2012	13:12 – 16:34	Toulouse-Toulouse	Gulf of Lion	Test flight
	V17*	22/06/2012	09:01 – 12:54	Toulouse-Toulouse	South-western France (over land) and the Atlantic Ocean	Test flight, biogenic emissions.
	V18*	26/06/2012	07:13 – 09:18	Toulouse-Bastia	Gulf of Genoa	Export of pollution from Northern Italy/Pô Valley, north-westerly winds
	V19	26/06/2012	10:42 – 13:46	Bastia-Toulouse	Gulf of Genoa	Export of pollution from Northern Italy/Pô Valley, north-westerly winds
	V20	27/06/2012	04:07 – 08:00	Toulouse-Nimes	Sea area south of Marseille/Toulon	Export of pollution during a Mistral-Tramontane event
	V21	27/06/2012	09:39 – 13:16	Nimes-Toulouse	Western coast of Corsica	Export of pollution from Northern Italy/Pô Valley, north-westerly winds
	V22	29/06/2012	05:13 – 08:50	Toulouse-Bastia	Eastern coast of Corsica	Dust outbreak
	V23	29/06/2012	10:13 – 14:12	Bastia-Toulouse	Eastern and western coasts of Corsica	Dust outbreak
	V24	03/07/2012	13:19 – 17:12	Toulouse-Toulouse	Sea area north-east of Barcelona	Export of pollution from Barcelona, westerly/south-westerly winds
	V25	04/07/2012	07:18 – 10:54	Toulouse-Toulouse	Sea area south of Marseille/Toulon	Follow of Barcelona pollution plumes
	V26	04/07/2012	15:25 – 18:36	Toulouse-Toulouse	Gulf of Lion	Follow of Barcelona pollution plumes
	V27	06/07/2012	08:00 – 11.55	Toulouse-Toulouse	Sea area south of Marseille	Export of pollution during a moderate Mistral-Tramontane event
	V28	06/07/2012	14:01 – 17:45	Toulouse-Toulouse	Sea area south of Nice/Toulon	Export of pollution during a moderate Mistral-Tramontane event
	V29*	07/07/2012	08:19 – 10:59	Toulouse-Nimes	Southern France (over land)	Biogenic emissions
	V30	07/07/2012	13:03 – 17:10	Nimes-Toulouse	Gulf of Genoa	Export of pollution during a moderate Mistral-Tramontane event
	V31	10/07/2012	13:41 – 17:21	Toulouse-Toulouse	Eastern coast of Spain	Characterization of pollution near coastal

						sources
	V32	11/07/2012	11:23 – 14:48	Toulouse-Toulouse	Southeastern coast of France and Gulf of Genoa	Characterization of pollution near coastal sources
SAFMED 2013	V46	24/07/2013	10:34 – 13:06	Genoa-Cagliari	Gulf of Genoa and eastern coast of Corsica and Sardinia	Characterization of pollution plumes in the Gulf of Genoa, Corsica, and Sardinia; westerly/south-westerly winds
	V47*	24/07/2013	14:21 – 16:29	Cagliari-Genoa	Eastern coast of Corsica and Sardinia and Gulf of Genoa	Characterization of pollution plumes in the Gulf of Genoa, Corsica, and Sardinia; westerly/south-westerly winds
	V48	25/07/2013	13:12 – 16:02	Genoa-Ersa	Gulf of Genoa	Characterization of pollution in the Gulf of Genoa; westerly/south-westerly winds
	V49	27/07/2013	11:08 – 13:07	Genoa-Alghero	Central Italy (over land)	Characterization of pollution in central Italy
	V50*	27/07/2013	15:33 – 16:48	Alghero-Genoa	Eastern coast of Corsica and Gulf of Genoa	Characterization of pollution plumes in the Gulf of Genoa, Corsica, and Sardinia; westerly/south-westerly winds + dust outbreak
	V51	30/07/2013	13:05 – 15:50	Genoa-Ersa	Gulf of Genoa	Characterization of pollution in the Gulf of Genoa; very low north/north-westerly winds
	V52	01/08/2013	12:03 – 15:24	Genoa-Alghero	Western coast of Corsica	Characterization of pollution in western Corsica; export of pollution from Northern Italy/Pô Valley; north-easterly winds

898
899 * = No vertical profiles performed during these flights.
900
901
902
903
904
905

Table 2. Comparison of the number concentrations dN_{Aitken} (0.004-0.1 µm) and dN_{Acc} (0.1-1.0 µm) observed during the TRAQA/SAFMED field campaigns with those reported in literature for continental Europe. All literature data refer to airborne measurements.

Atmospheric layer	Parameter	TRAQA/SAFMED	Literature over continental Europe
Free troposphere (FT)	dN_{Aitken} (scm^{-3})	0-19250	812-9149[b]; 0-980[e]
	dN_{Acc} (scm^{-3})	34-3233	20-80[a]; 25-85[e]; 0-500[f]
Boundary layer (BL)	dN_{Aitken} (scm^{-3})	4-22471	1037-31370[b]; 1000-20000[c]; 0-30000[d]; 0-19000[e]
	dN_{Acc} (scm^{-3})	90-3215	70-560[a]; 10-50[c]; 400-1200[e]; 0-2000[f]

[a] Petzold et al. (2002), Central Europe, July-August 1998; size range dN_{Acc} (>0.15 µm)

[b] Mallet et al. (2005), Southeastern France, June 2001; size range dN_{Aitken} (0.006-0.6 µm)

[c] Wiegner et al. (2006), Germany, May 2003; ; size range dN_{Aitken} (>0.01 µm), dN_{Acc} (>0.3 µm)

[d] Junkermann (2009), Po Valley, July-August 2002 and September-October 2003; ; size range dN_{Aitken} (>0.01 µm)

[e] Hamburger et al. (2012), central Europe, May 2008; size range dN_{Aitken} (0.004-0.15 µm), dN_{Acc} (>0.15 µm)

[f] Highwood et al. (2012), central Europe, May 2008; size range dN_{Aitken} (0.004-0.15 µm), dN_{Acc} (>0.15 µm)

Figures

Figure 1. (Upper panel) Flight trajectories of the TRAQA (20 June - 13 July 2012) and the SAFMED (24 July - 1 August 2013) campaigns. The aircraft was based in Toulouse (43°36'N, 1°26'E, France) during TRAQA and in Genoa (44°24'N, 8°55'E, Italy) during SAFMED. (Lower panel) Zoom on the investigated area and geographical position of the different vertical soundings analysed in this paper. The position of the three AERONET stations of Barcelona, Frioul, and Ersa considered in this study is also shown.

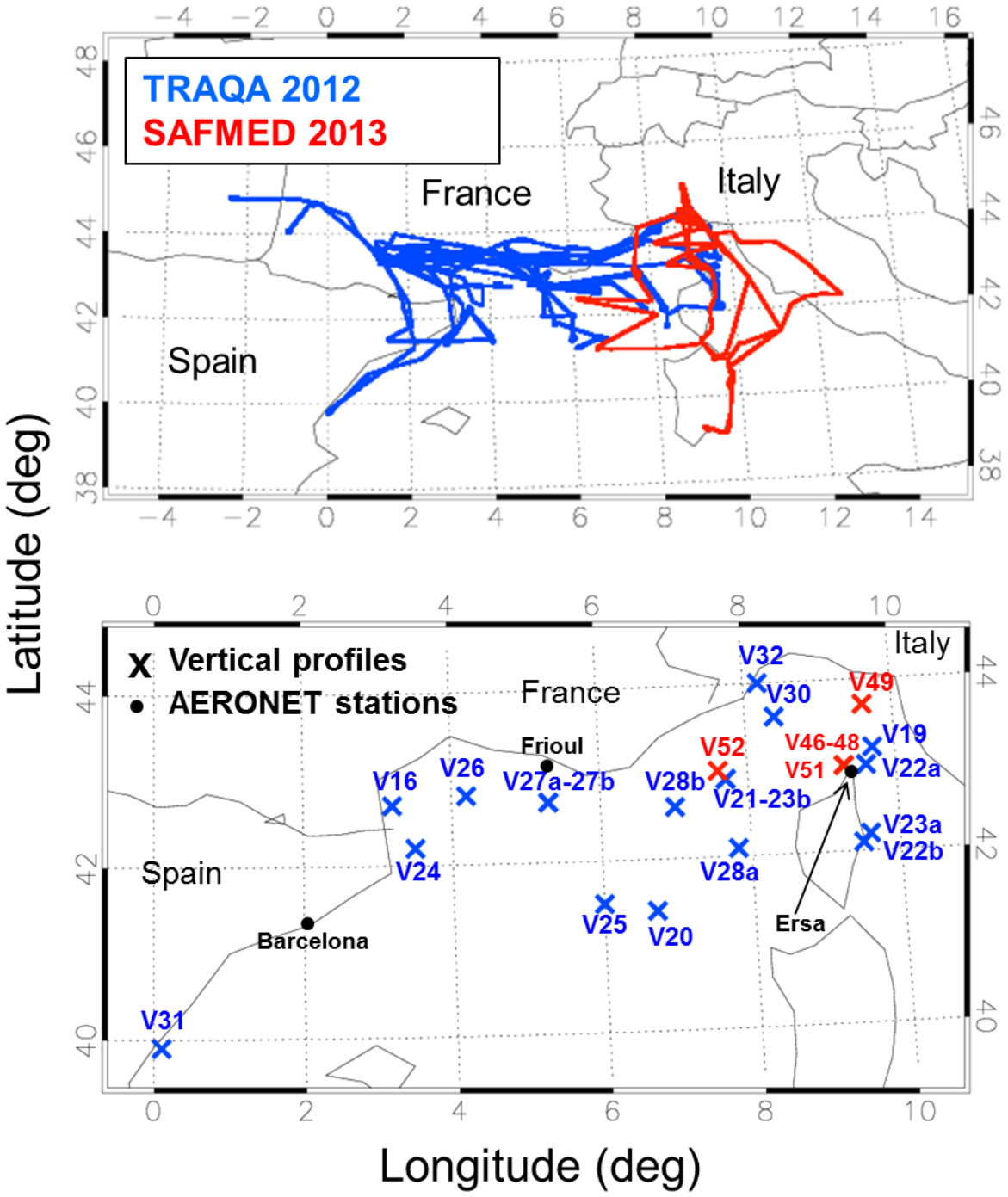

Figure 2. Aerosol optical depth at 440 nm (τ) and Ångström exponent (α) measured at the Barcelona, Frioul, and Ersa AERONET stations during the TRAQA 2012 (left panels) and the SAFMED 2013 (right panels) campaigns. The time period for the different plots is ±10 days around the beginning/end of the two campaigns (data for the Barcelona station are not available over the entire period for 2012). The label D indicates the days affected by Saharan dust.

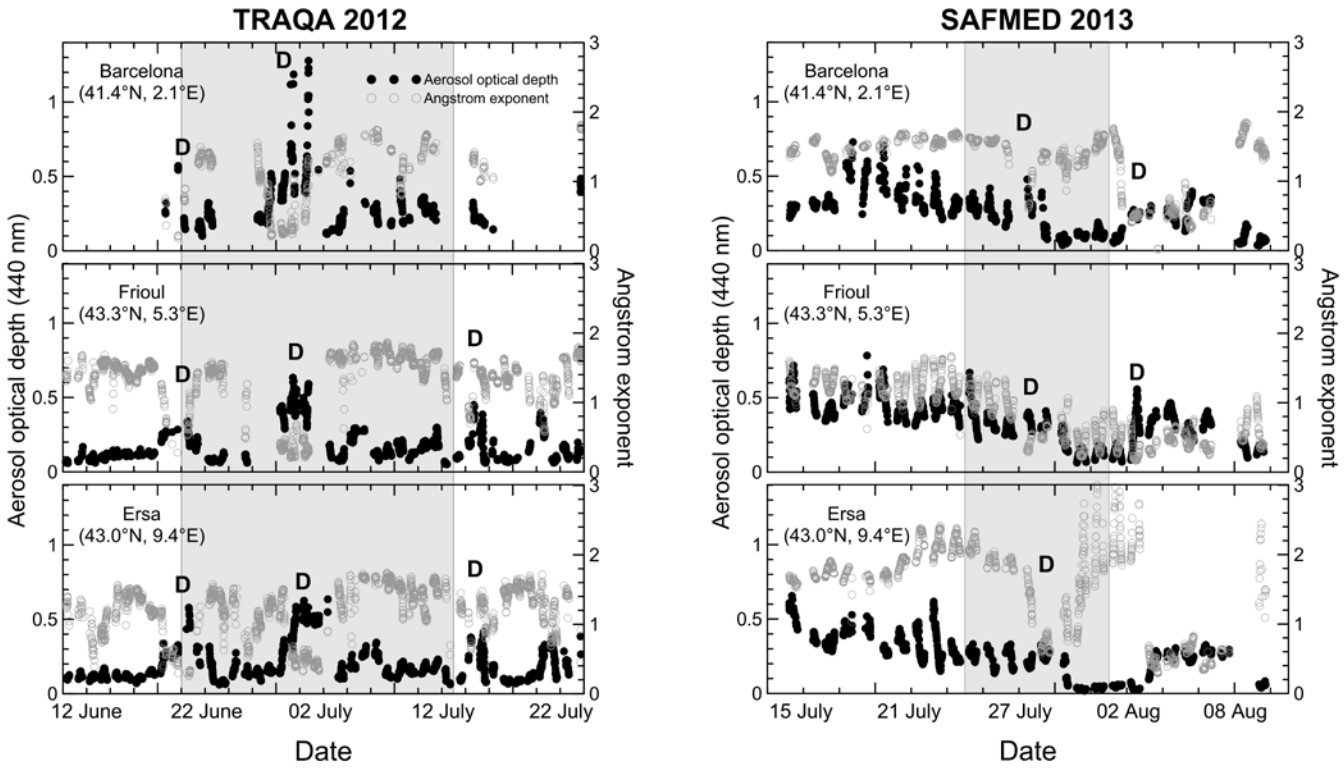

975 **Figure 3.** Example of wind maps at 925 mbar for 26 June and 3 July 2012. The maps are obtained
976 from the WRF-Chem model (Weather Research and Forecasting – Chemistry) at 10-km horizontal
977 resolution.
978

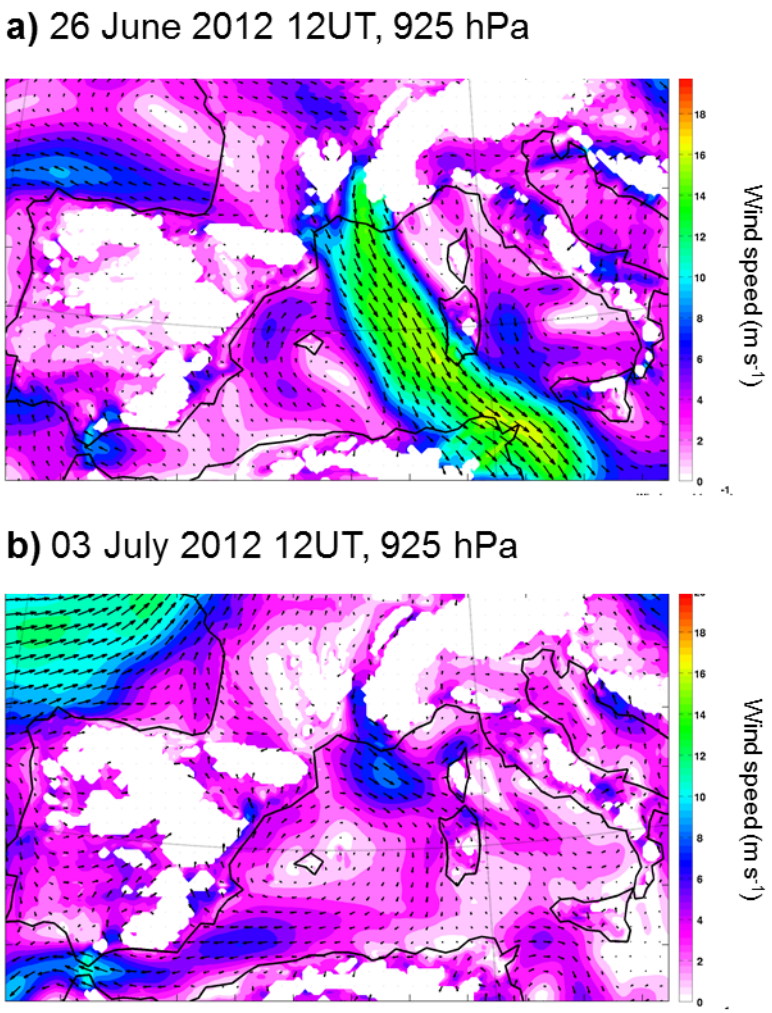

979
980
981
982
983
984
985
986
987
988
989
990

Figure 4. (Left) Scattering coefficient σ_s at 450, 550, and 700 nm versus the scattering Ångstrom exponent α_s. Cases with extremely negative (<−2) and positive (>4) values of α_s are always related with very low scattering coefficients, and are likely due to instrumental noise under low scattering conditions. (Right) Frequency of occurrence of α_s obtained considering vertical profiles data from all TRAQA and SAFMED flights.

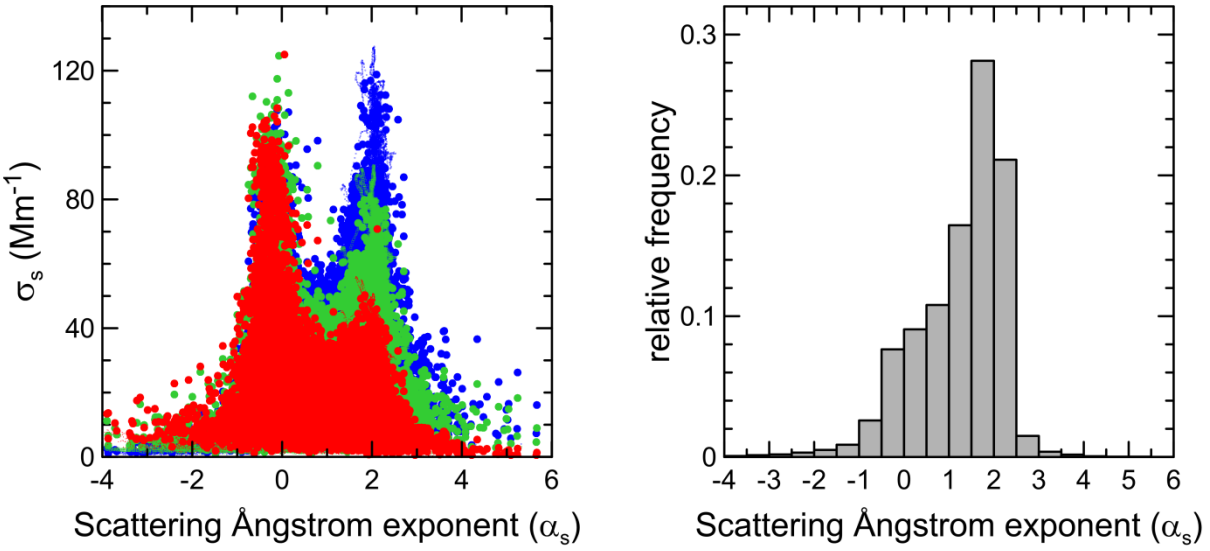

Figure 5. Box and whisker plot of the aerosol scattering coefficient (σ_s) at 450, 550, and 700 nm, particle concentration in the Aitken (dN_{Aitken}) and accumulation (dN_{Acc}) modes, and CO and O_3 measured within pollution plumes in the boundary layer (BL) and in the free troposphere (FT).

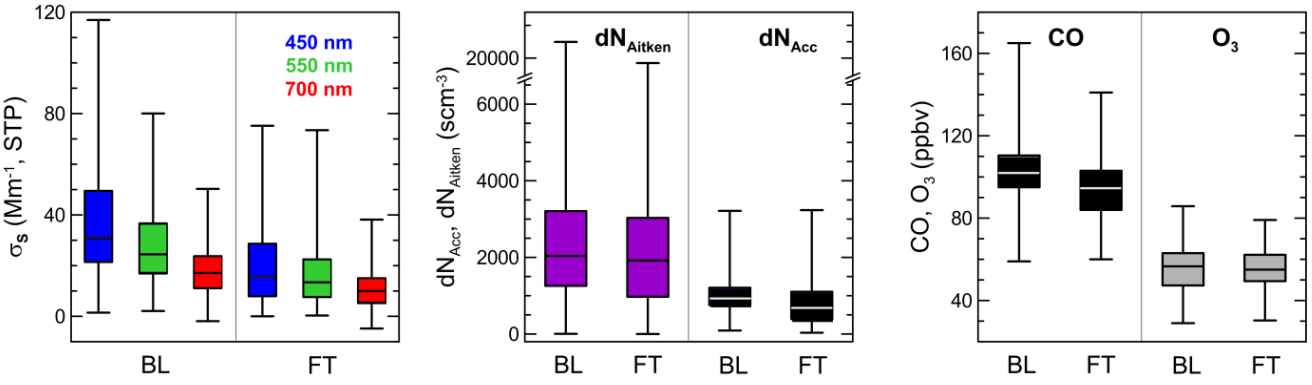

Figure 6. Vertical profiles of the spectral scattering coefficient σ_s at 450, 550, and 700 nm and particle number concentration in the 0.1-1.0 µm (dN_{Acc}) and 1.0-4.0 µm (dN_{Coarse}^{*}) diameter ranges observed during TRAQA and SAFMED. Data are reported at STP (standard temperature and pressure, T =293.15 K and P=1013.25 hPa). The heights of the top of the marine aerosol boundary layer (MABL) and planetary boundary layer (BL) estimated from the meteorological profiles are also indicated in the plots. The label D is used to identify the aerosol layers affected by Saharan dust. For certain flights (V22, V23, V27, and V28) two vertical soundings were performed; the letters "a" and "b" after the flight number in this plot specify if the considered data are taken from the first or the second sounding, respectively.
(* data for dN_{Coarse} are multiplied by 100 in the plot).

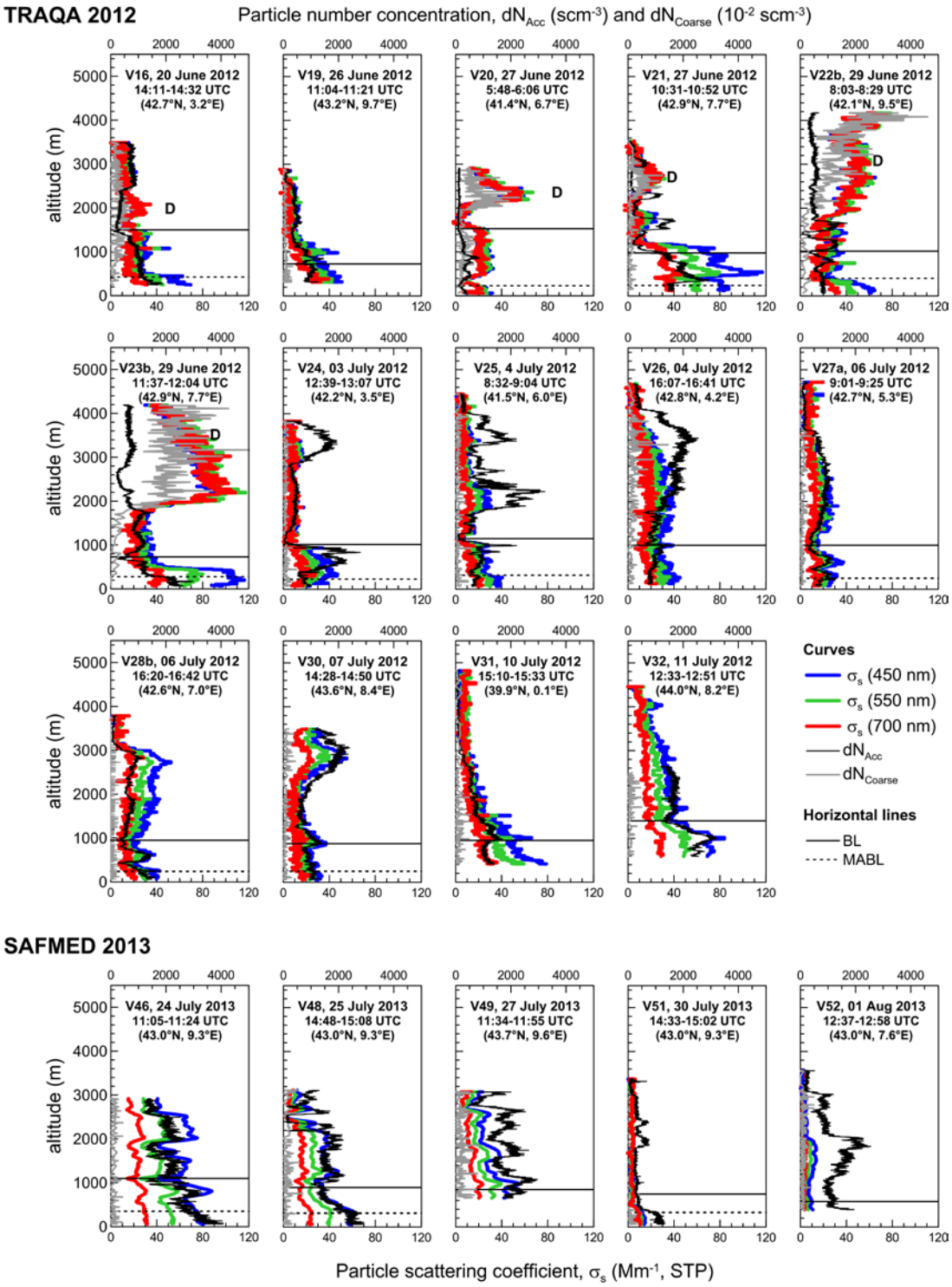

Figure 7. O_3 versus CO in the boundary layer (BL) and the free troposphere (FT) for all TRAQA and SAFMED vertical profiles (dust observations excluded).

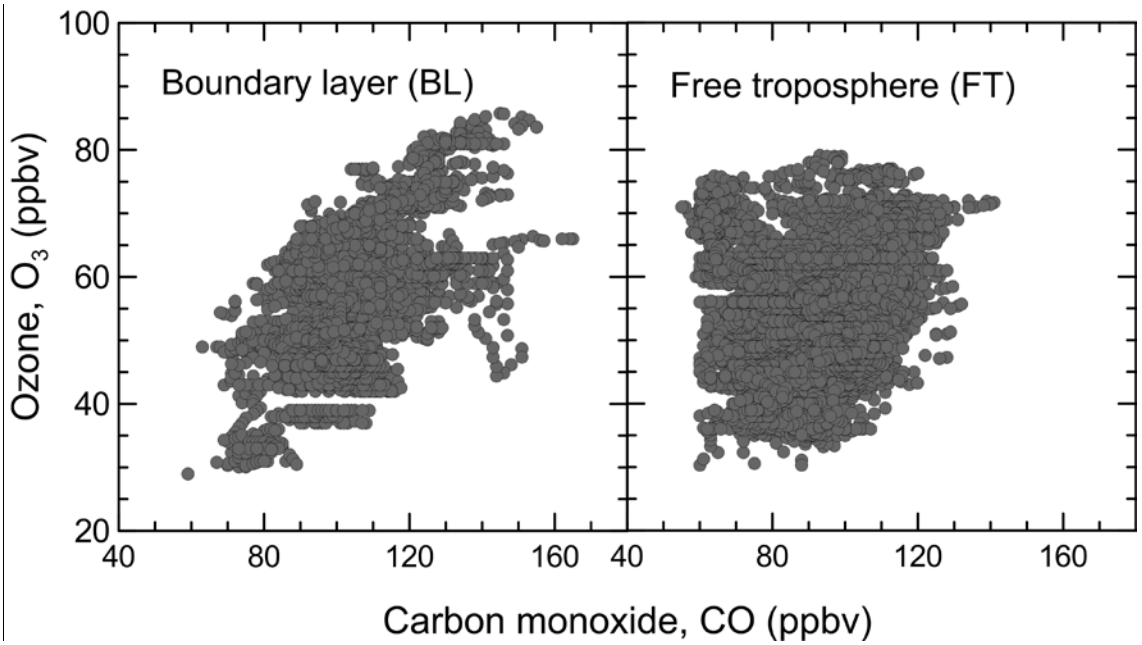

Figure 8. Aerosol and trace gases vertical profiles for flights V19 (export from northern Italy/Po Valley), V20 (Mistral event), and V24 (export from the Barcelona area). The plots show the: (a) spectral scattering coefficient σ_s at 450, 550, and 700 nm (blue, green, and red lines, respectively), temperature (T, black line), and relative humidity (RH, light blue line); (b) particle number concentration in the 0.004-0.1 µm (dN_{Aitken}, purple line) and 0.1-1.0 µm (dN_{Acc}, black line) diameter ranges, (c) CO (black dots) and O_3 (grey dots) mixing ratios, (d) ozone enhancement factor $\Delta O_3/\Delta CO$ (grey dots) and Aitken to accumulation ratio dN_{Aitken}/dN_{Acc} (pink dots) and (e) horizontal wind vector. The heights of the top of the MABL (dotted line) and BL (solid line) are also indicated.

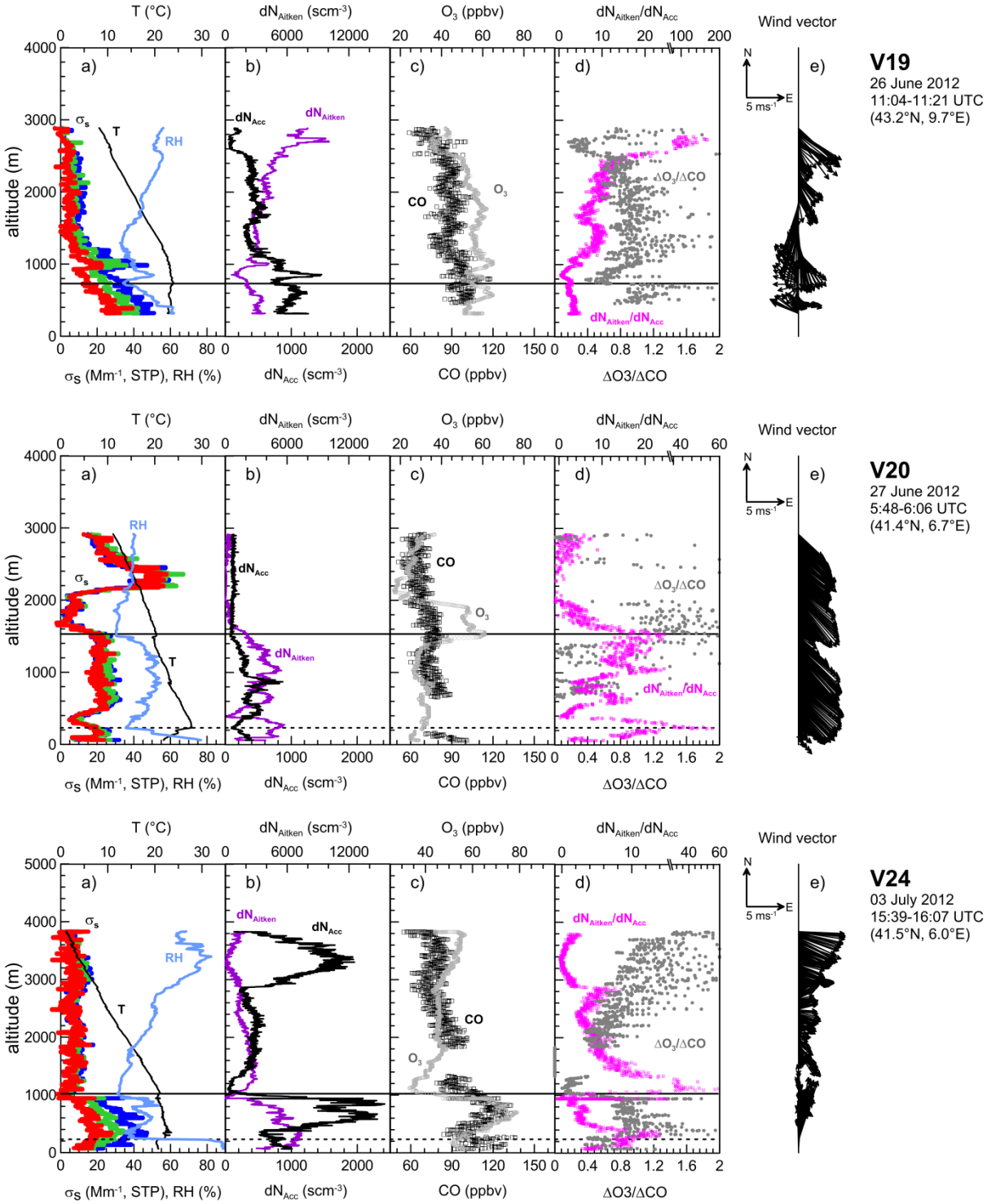

Figure 9. Five-days backward air mass trajectories for the V19, V20, and V24 flights calculated with the FLEXTRA model. The upper panel shows the trajectories over an extended latitude-longitude region, while the central panel zooms on the Western Mediterranean area. The altitude of the air masses and its temporal evolution along the five days trajectories is reported in the lower panel of each plot.

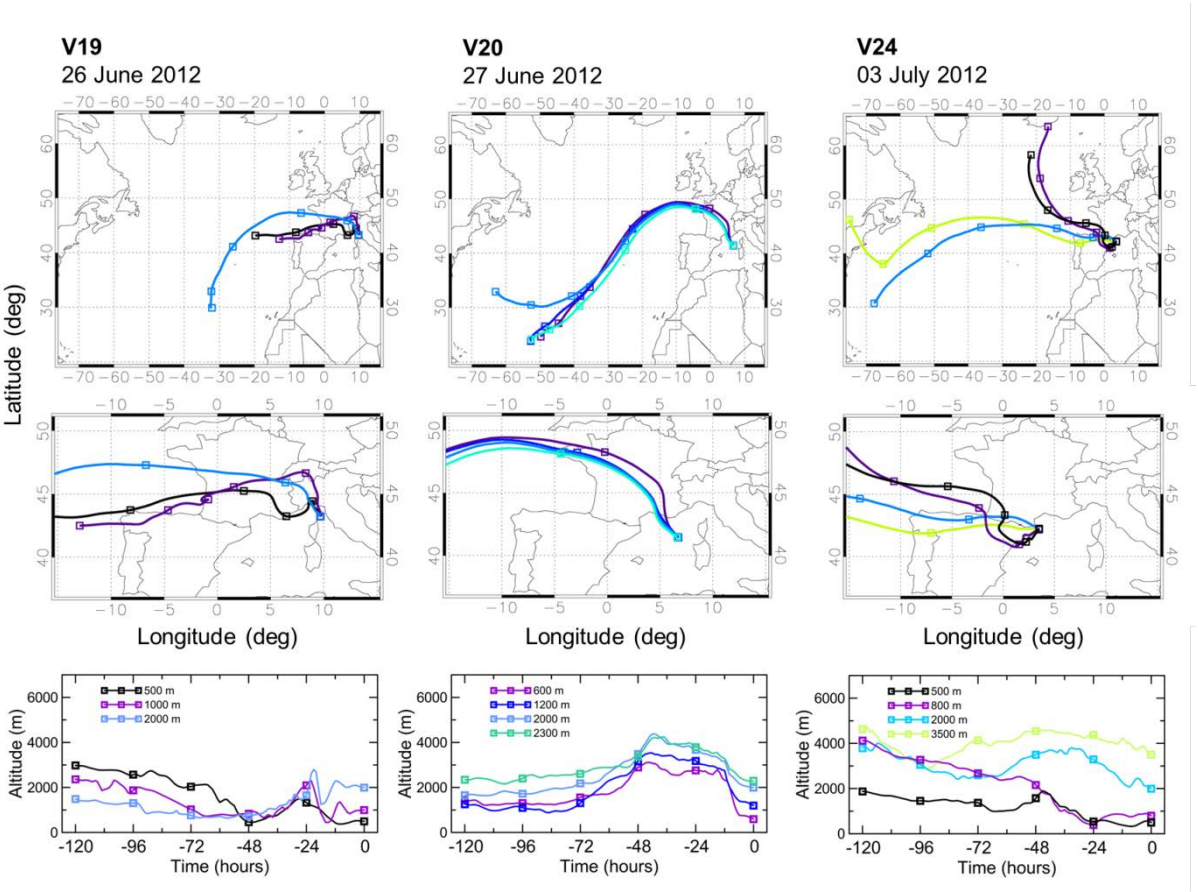

Figure 10. Vertical profiles of the accumulation and Aitken particle concentrations (dN_{Acc}, black line, and dN_{Aitken}, purple line), CO (black dots), O_3 (grey dots), and gradient Richardson number (Ri, green line) for flights a) V31, b) V28, c) V19, d) V26 and e) V23b. The horizontal lines indicate the height of the marine boundary layer MABL (dotted line) and the planetary boundary layer BL (continuous line), while the vertical lines indicate Ri_{crit}=0.25 and Ri=1 (continuous and dashed lines, respectively).